MICROEMULSION ASSISTED SYNTHESIS OF MAGNETITE NANOPARTICLES

Dissertation Submitted for Partial Fulfilment of Requirements for Master of Science Degree in Chemistry

By

Gunakhar Devkota

Exam Roll No.: CHE-1023 / 074

T.U. Regd. No.: 5-2-37-2247-2013

Submitted to

Central Department of Chemistry

Institute of Science and Technology (IOST)

Tribhuvan University, Kirtipur

Kathmandu, Nepal

2022

BOARD OF EXAMINER AND CERTIFICATE OF APPROVAL

This dissertation entitled **"MICROEMULSION ASSISTED SYNTHESIS OF MAGNETITE NANOPARTICLES"** by Mr. Gunakhar Devkota under the supervision of Prof. Dr. Rameshwar Adhikari, Central Department of Chemistry, Tribhuvan University, Nepal, is hereby submitted for the partial fulfilment of the Master of Science (M. Sc.) Degree in Chemistry. This dissertation has not been submitted to any other university or institution previously for the award of a degree.

Supervisor
Prof. Dr. Rameshwar Adhikari
Central Department of Chemistry,
Tribhuvan University

Internal Examiner
Asst. Prof. Dr. Kshama Parajuli,
Central Department of Chemistry,
Tribhuvan University

External Examiner
Assoc. Prof. Dr. Sharmila Pradhan Amatya,
Department of Chemistry,
Amrit Science College

Prof. Dr. Ram Chandra Basnyat
Head of the Department
Central Department of Chemistry,
Tribhuvan University

Central Department of Chemistry
Institute of Science and Technology
Tribhuvan University, Kirtipur,
Kathmandu, Nepal

LETTER OF RECOMMENDATION

This is to certify that the dissertation work entitled **"MICROEMULSION ASSISTED SYNTHESIS OF MAGNETITE NANOPARTICLES"** submitted by Mr. Gunakhar Devkota has been carried out under my supervision. The entire study was based on the results of his original research work; and as far as my knowledge, this work has not been submitted for any other academic degree. I, therefore, recommend this dissertation to be accepted for the partial fulfilment of Master of Science in Chemistry from Tribhuvan University, Kathmandu, Nepal.

(Supervisor)

Prof. Dr. Rameshwar Adhikari

Central Department of Chemistry,

Tribhuvan University, Kathmandu, Nepal

Date:

DECLARATION

I, Gunakhar Devkota, hereby declare that the work presented herein is genuine work done originally by me and has not been published or submitted elsewhere for the requirement of a degree program. Any literature, data or work done by others and cited in this dissertation have been given due acknowledgement and listed in the reference section.

Gunakhar Devkota
Central Department of Chemistry,
Tribhuvan University, Kathmandu, Nepal

Date:

ACKNOWLEDGEMENT

First of all, I would like to express my sincere gratitude to my respected supervisor, Prof. Dr. Rameshwar Adhikari, Central Department of Chemistry, Tribhuvan University, for his guidance, advice, encouragement and continuous support throughout the work.

I would like to extend my gratitude to Prof. Dr. Ram Chandra Basnyat, Head, Central Department of Chemistry, Tribhuvan University for providing letters that had been submitted in NYC.

My special thanks to all teachers and administrative staff of the Research Centre for Applied Science and Technology (RECAST) and Central Department of Chemistry, Tribhuvan University for their kind co-operation during my lab work.

My sincere thanks to those who have provided me with experimental training and assistance throughout this study, most notably Dr. Sven Henning and Mr. Achyut Nepal for their assistance with Scanning Electron Microscopy (SEM)**,** Nepal Academy of Science and Technology **(**NAST) for assistance with X-ray diffraction (XRD)**,** Dr. Khag Raj Sharma (Central Department of Chemistry) for his assistance with Fourier Transform Infrared (FTIR) Spectroscopy and also for Mr. Ramesh Puri for his gentle assistance with Ultraviolet-Visible (UV-Vis) analysis. Thanks to University Grant Commission (UGC) for providing FTIR facilities to RECAST. I wish to record my gratitude to my parents and all the research scholars who have directly or indirectly supported me throughout this project, most notably Dr. Shankar Khatiwada, Dr. Subin Adhikari, Dr. Sabina Shrestha, Dr. Rakshya Dangol, Ms. Asmita Khanal, Mr. Bidit Lamsal, Mr. Tika Ram Bhandari, Mr. Ghanashyam Chaudhary, Mrs. Prasamsha Pant, Mrs. Elina Maharjan, Ms. Deepti Bhusal as well as all the members of RECAST for their constant help and support.

I would like to acknowledge National Youth Council (NYC), Sanothimi, Bhaktapur for the financial support required during this work. I also extend my heartiest appreciation to all the people who have made it possible for me to complete this thesis.

ABSTRACT

Microemulsion techniques have been widely used to prepare nanoparticles (NPs) of controlled shapes and dimensions. Magnetite nanoparticles (Fe_3O_4) of various sizes were synthesized using the water in oil (w/o) microemulsion as nano-reactors. Commonly available mustard and soybean oils were used beside hexane as oil phases for the synthesis. The effect of the oil phase on the structure, optical band gap and morphology of the nanoparticles were studied. The X-ray diffractogram of each of the samples showed a well-defined crystalline phase with no effect of the oil phase in their crystal structure. UV spectra of the samples showed the surface plasmon resonance at nearly the same value of 220 nm with different bandgap energies. The average diameter of the spheroid particles was found to be 57 nm, 33 nm and 24 nm on using hexane, mustard oil, and soybean oil as organic phases, respectively. This way, the nanoparticles of variable sizes could be prepared by changing the oil phase in the microemulsion.

Keywords: Magnetite, Microemulsion, Soybean oil, Sunflower oil, Optical band gap

सारांश

आजकल माइक्रोईमल्सन नामक विधिको प्रयोगद्वारा निश्चित आकार-प्रकार र आयाम भएका नानोकणिकाहरु तयार गर्ने प्रविधिको बिकाश भएको पाईन्छ । यो अनुसंधानको क्रममा "तेल भित्र पानी (तेल[पानी])" कोटीको माइक्रोईमल्सनलाई नानोप्रतिक्रियाशालाको रुपमा उपयोग गरेर विविध आकारका म्याग्नेटाइट नामक चुम्बकीय गुणयुक्त नानोकणिकाहरु संश्लेषण गरिएको थियो । यो अध्ययनमा तैलीय बस्तुको रुपमा हेक्जेन तथा तोरी र भटमासको तेललाई प्रयोग गरि तिनीहरुले नानोकणिकाको बनोट, आकार-प्रकार तथा अप्टिकल ब्याण्ड ग्यापमा पार्ने प्रभावको बारेमा विश्लेषण गरिएको थियो । प्राप्त नानोकणिकाहरुको नमुनामा गरिएको एक्स-रे विवर्तनले ति सवै नमुनामा मणीभिय संरचना विद्यमान भएको तथा तिनीहरुको आन्तरिक रचनामा तैलीय बस्तुको कुनै प्रभाव नरहेको पाईयो । प्रत्येक नमुनाको परावैजनी-दृश्य-पटको अध्ययन गर्दा तिनीहरुमा असमान अप्टिकल ब्याण्ड ग्याप भएका र झन्डै २२० नानोमीटरमा प्रकाशको अधिक शोषण गर्ने नानोकणिकाहरु बनेको थाहा पाईयो । साथै हेक्जेन तथा तोरी र भटमासको तेललाई तैलीय बस्तुको रुपमा प्रयोग गर्दा क्रमसः ५७ नानोमीटर, ३३ नानोमीटर र २४ नानोमीटर ब्यासका गोलाकार नानोकणिकाहरु बनेको समेत निर्क्यौल गरियो । यसरी, माइक्रोईमल्सनको बनौटमा तैलीय बस्तुको विविधिकरण गरेर विभिन्न आयतनका गोलाकार नानोकणिकाहरु तयार गर्न सकिन्छ भन्ने निष्कर्षमा पुगियो ।

ACRONYMS AND ABBREVIATIONS

BSI	British Standards Institution
CVD	Chemical Vapor Deposition
FTIR	Fourier Transform Infrared
FWHM	Full Width at Half Maximum
ISO	International Organization for Standardization
MNPs	Magnetite Nanoparticles
MNPs-$_{Hex}$	Magnetite Nanoparticles Synthesized Using Hexane as Oil Phase
MNPs-$_{Soya}$	Magnetite Nanoparticles Synthesized Using Soybean Oil as Oil Phase
MNPs-$_{Must}$	Magnetite Nanoparticles Synthesized Using Mustard Oil as Oil Phase
NPs	Nanoparticles
PVD	Physical Vapor Deposition
SCCP	Scientific Committee on Consumer Product
SEM	Scanning Electron Microscopy
XRD	X-ray Diffraction

LIST OF FIGURES

Figure 1.1: Scheme showing the particles having diameter ranging from sub nanoscopic scale to microscopic and macroscopic scales

Figure 1.2: Lycurgus cup with unique optical property

Figure 1.3: Unit cell of magnetite

Figure 2.1: Antimicrobial mechanism of SeO_2 nanoparticle

Figure 2.2: Change in optical property due to quantum confinement effect

Figure 2.3: Surface plasmon resonance of gold nanoparticle

Figure 2.4: Sol-gel technique for nanoparticle synthesis

Figure 2.5: Microemulsion technique for nanoparticle synthesis

Figure 2.6: Illustration of a magnetic adsorption process

Figure 2.7: Illustration of a typical magnetic hyperthermia therapy process

Figure 3.1: Photographs showing the change in transparency of solution due to microemulsion formation: a) translucent solution before stirring, and b) transparent solution after stirring for 30 min

Figure 3.2: Photographs showing preparation of MNP_s: a) the apparatus showing arrangement of inert gas environment during synthesis, and b) MNPs containing round-bottom flask showing black precipitate

Figure 3.3: Illustration for preliminary study of physical properties of synthesized powder: a) magnetic property, and b) Tyndall effect

Figure 4.1: Photographs showing MNPs: a) physical appearance of MNPs, and b) magnetic nature of particles shown by their attraction to magnetic fish

Figure 4.2: Photographs showing optical property and particle morphology: a) scattering of laser by MNPs colloidal solution, and b) optical micrograph of MNPs deposited on glass slide

Figure 4.3: Surface plasmon absorption and tauc plot for $MNPs\text{-}_{Hex}$

Figure 4.4: Surface plasmon absorption and tauc plot for $MNPs\text{-}_{Must}$

Figure 4.5: Surface plasmon absorption and tauc plot for $MNPs\text{-}_{Soya}$

Figure 4.6: FTIR spectra of Fe_3O_4 NPs

Figure 4.7: XRD patterns of various MNPs samples

Figure 4.8: SEM micrographs of $MNPs\text{-}_{Hex}$: a) High pressure magnification, b) Low pressure magnification, and c) Size distribution curve

Figure 4.9: SEM micrographs of MNPs-$_{Must}$: a) High pressure magnification, b) Low pressure magnification, and c) Size distribution curve

Figure 4.10: SEM micrographs of MNPs-$_{Soya}$: a) Higher magnification, b) Lower magnification, and c) Size distribution curve

Figure 4.11: Morphology comparison of MNPs: a) prepared by sol-gel method (Xu et al., 2007), and b) prepared using w/o microemulsion

LIST OF TABLES

Table 1.1: Nanotechnology in nature

Table 1.2: Historical development in nanochemistry

Table 2.1: Comparison of properties of nickel in microscopic and nanoscopic ranges

Table 2.2: Classification of iron oxide

Table 2.3: Different methods for nanoparticle synthesis

Table 2.4: Comparison of different methods for the fabrication of NPs

Table 2.5: Different approaches for MNPs synthesis

Table 4.1: Absorption peak and band gap energy of different MNPs

Table 4.2: Crystallite size of MNPs prepared by various methods

TABLE OF CONTENT

LETTER OF RECOMMENDATION ii

DECLARATION iii

ACKNOWLEDGEMENT iv

ABSTRACT v

सारांश vi

ACRONYMS AND ABBREVIATIONS vii

LIST OF FIGURES viii

LIST OF TABLES x

TABLE OF CONTENT xi

CHAPTER 1 1

INTRODUCTION 1

1.1 Definitions of Nanomaterials and Nanotechnology 1

1.2 Historical Development 3

1.3 Magnetite Nanoparticles 4

1.4 Objectives 6

CHAPTER 2 7

LITERATURE SURVEY 7

2.1 Unique Properties of Nanostructured Materials 7

2.1.1 Antimicrobial properties: 8

2.1.2 Quantum confinement: 8

2.1.3 Surface plasmon resonance (SPR): 9

2.2 Iron Oxide Nanoparticles and Their Properties 10

2.2.1 Various forms of iron oxides 10

2.2.2 Methods for producing nanoparticles 11

2.2.3 Applications of magnetite nanoparticles 17

I. Magnetite nanoparticles in heavy metal removal 17

II. Magnetite nanoparticles in biomedical application 18

III. Magnetite nanoparticles in electrical application 20

CHAPTER 3 21

EXPERIMENTAL 21

3.1 Materials 21

3.2 Preparation of Solutions 21
3.2.1 Preparation of microemulsions 21
3.2.2 Preparation of microemulsion containing the salt precursor: 22
3.2.3 Preparation of microemulsion containing the precipitating agent: 22
3.3 Preparation of Magnetite Nanoparticles (MNPs): 23
3.4 Characterization Methods 24
3.4.1 Preliminary characterization 24
3.4.2 X-Ray powder diffraction (XRD) 25
3.4.3 Fourier transform infrared (FTIR) spectroscopy 25
3.4.4 Ultraviolet-visible (UV-Vis) spectroscopy 26
3.4.5 Scanning electron microscopy (SEM) 26
CHAPTER 4 27
4.1 Preliminary Characterization 27
4.2 Chemical Characterization 28
4.2.1 Ultraviolet-visible (UV-Vis) spectroscopy and Tauc plots 28
4.2.2 Fourier transform infrared spectroscopy (FTIR) 32
4.3 Structural Characterization 33
4.3.1 Study of crystal structure using x-ray diffraction 33
4.3.2 Study of size and morphology using scanning electron microscopy 34
CHAPTER 5 38
CONCLUSION AND PERSPECTIVES 38
References 39

CHAPTER 1

INTRODUCTION

1.1 Definitions of Nanomaterials and Nanotechnology

International organization of standardization (ISO) has defined a nanoparticle as "The particle having its diameter in between 1 nm to 100 nm is nanoparticle" (Boholm & Arvidsson, 2016). According to British Standards Institution (BSI), "If all the field or diameter of the particle is in nanoscopic range then the particle is nanoparticle" (Jeevanandam et al., 2018). Scientific Committee on Consumer Products (SCCP) defined a nanoparticle (NP) as "The particle whose at least one dimension is in the nanoscale range". Thus, nanochemistry deals with the study of the synthesis and application of the material whose dimension lies in the nanoscopic range (Schaming & Remita, 2015).

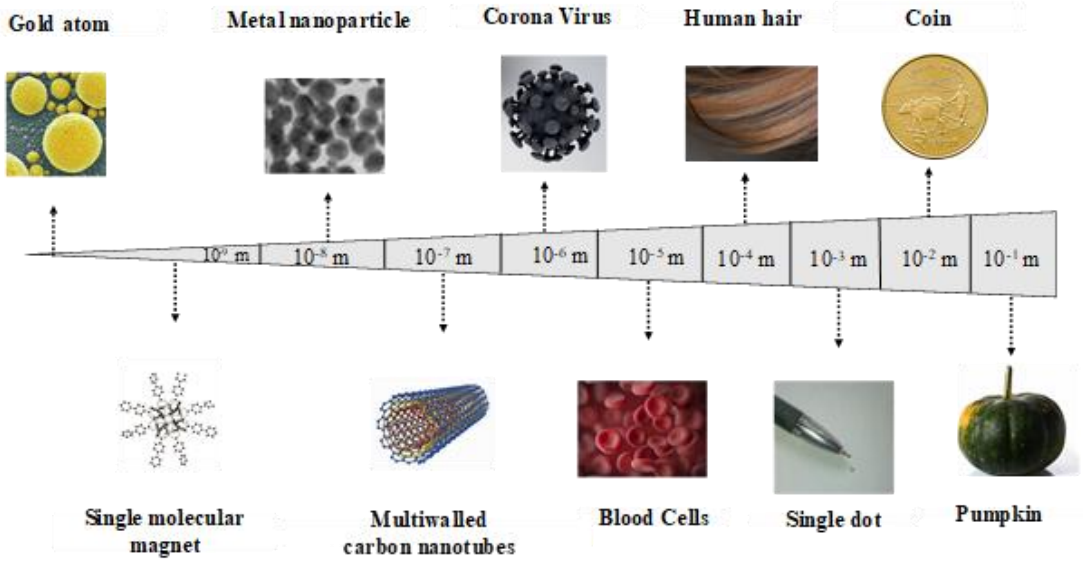

Figure 1.1: Scheme showing the particles having a diameter ranging from sub nanoscopic scale to microscopic and macroscopic scales

As shown in Figure 1.1, the size of red blood cells and viruses is mesoscopic in size visible by an optical microscope, whereas atoms and molecules have a size less than 1 nm. The size of nanoparticles is between these two extremes i.e. larger than molecular level but for smaller than macroscopic materials. Nanotechnology thus encompasses

the science of contrary, manipulating and applying objects with dimensions between 1 nm and 100 nm.

The term nanotechnology was first introduced by Prof. Norio Taniguchi in order to explain the "Processing of separation, consolidation, and deformation of materials by one atom or one molecule" (Mehnath et al., 2021). The International Union of Pure and Applied Chemistry (IUPAC) has defined nanotechnology as the "Manipulation of matter on an atomic and molecular scale" (Jones et al., 2020). The definition of nanotechnology as proposed by the National Aeronautics and Space Administration (NASA) is, "The creation of functional materials, devices and systems through control of matter on the nanometer length scale 1 nm to 100 nm, and exploitation of novel phenomena and properties such as physical, chemical, biological at that length scale" (Mehnath et al., 2021).

Nature is an inspirational source for many scientific researches and has also produced several nanostructured materials that make life possible for various biomass. A simple example of such material is the smallest unit of life, the cell. A cell membrane is a part of the cell that has its dimension in the nanoscopic range and is considered a one-dimensional nanomaterial. Some other natural nanoscale phenomena and mechanisms are summarized in Table 1.1.

Table 1.1: Some nanoscale phenomena and mechanisms observed in various living organelles and organisms (Jeevanandam et al., 2018)

Natural Technologist	**Functions**
Cell Organelles	Basic metabolism of a living organism
Chlorophyll	Photosynthesis
Web spinning spider	Web synthesis that can resist light and water (strongest natural fiber)
Gecko	Able to walk on the wall (anti-gravity)
Lotus leaf	Self-cleaning action
Water strider	Able to walk on water

1.2 Historical Development

Nanotechnology has been used by humans since ancient times. During the Fourth century Romans used nanomaterials to create swords with high strength and flexibility. These swords consisted of 1.5% carbon in the form of nanotubes (Deshmukh, 2019). Similarly, microscopic analysis of Damascus steel swords made in the Fifth century showed the presence of carbon nanotubes that provided them with high strength. The strength of such steel was so great that it was capable to split a metal helmet in a single shot (Murty et al., 2013).

The famous Lycurgus Cup of the Fourth century was made of glass, contained gold-silver alloyed NPs which were distributed in such a way that the glass looks green in reflected light (Figure 1.2a) but, when light passes through the cup it reveals a brilliant red color as shown in Figure 1.2b (Deshmukh, 2019).

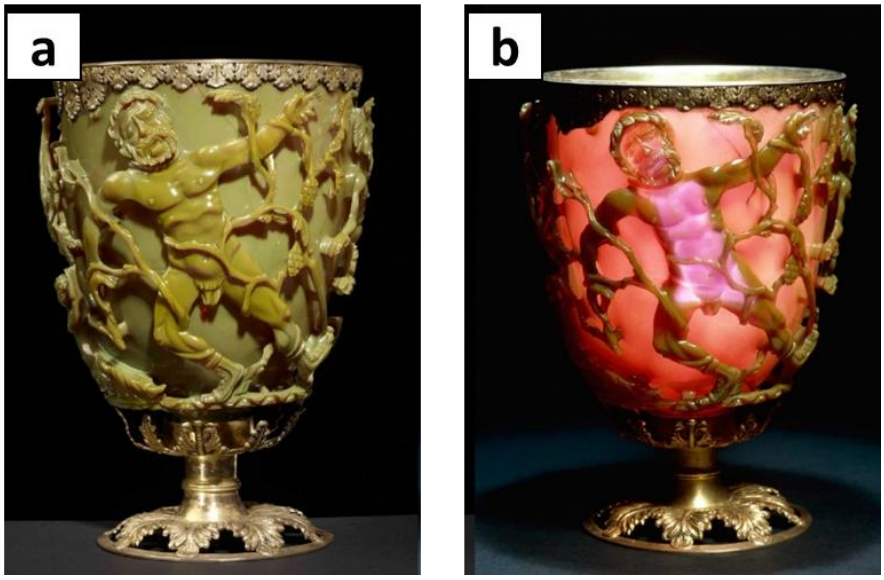

Figure 1.2: Lycurgus Cup with unique optical property (Freestone et al., 2008)

One of the chief reasons for the attraction to watching nanoparticles' research is due to their fascinating optical properties. Different metal nanoparticles show different colours due to which they can be used in decoration and paints. One of the most widely used nanoparticles was of gold in the size range of 20 nm which showed wine -red colour. Similarly, silver nanoparticle in the same size range is grey while platinum appears black (Schaming & Remita, 2015).

In 1857, by reducing the aqueous solution of complex salt of gold with phosphorous in presence of carbon disulphide, Faraday was successful to produce gold NPs in the laboratory, colloidal solution of gold, as those were called then. After this, many scientists tried to study these size depending properties. However, the lack of analytical instruments made it difficult to establish the size-dependent properties in the past. Rapid development in the field of nanotechnology was only possible after the discovery of the TEM in 1931 by M. Knoll and E. Ruska and then of STM in 1981 by G. Binnig and H. Rohrer. This has enabled scientists to develop several metallic, non-metallic as well as composite nanomaterials that have potential applications in different fields.

Some major contributions made by different scientists to nanochemistry development are summarized in Table 1.2.

Table 1.2: Historical development in nanochemistry (Schaming & Remita, 2015; Toumey, 2009)

Year	Breakthrough events	Scientist
1857	Synthesis of gold nanoparticle	M. Faraday
1900	There may be a tiny particle that obey their own law	M. Planks and A. Einstein
1902	Concept of surface plasmon resonance	R.W. Wood
1931	Discovery of TEM	M. Knoll and E. Ruska
1937	Discovery of SEM	M. V. Ardenne
1959	A lecture on "There is plenty of room at the bottom"	R. Feynman
1974	The term nanotechnology was introduced	N. Taniguchi
1980	Discovery of buckminster fullerene	R. E. Smalley
1981	Discovery of STM	G. Binnig and H. Rohrer
1986	The term "Molecular Nanotechnology" was introduced	E. Drexler
1991	The term "Nanomedicine" was introduced	Reported by (Min et al., 2015)
1991	Discovery of carbon nanotube	S. Iijima

1.3 Magnetite Nanoparticles

Ferrous-ferric oxide, commonly called magnetite is one of the main ores of iron. It has a molecular formula of Fe_3O_4 with the chemical composition of $Fe^{+2}\ Fe^{+3}{}_2\ O^{-2}{}_4$ and is mostly found in rocks. It is ferri-magnetic i.e. can be attracted to a magnet and become a permanent magnet. Lodestone, a naturally-magnetized piece of magnetite, was used by early people to discover the magnet and magnetic properties. The IUPAC

name for magnetite is iron (II,III) oxide and is the most magnetic naturally occurring mineral on earth (Morel et al., 2013). Almost all of the naturally occurring crystalline rocks and sedimentary rocks contain magnetite. Iron oxide ore with more than 70% of magnetite is considered to be a valuable source of iron. Such ores have been used for the extraction of iron since ancient times (Fleet, 1981).

Magnetite has an inverse spinel structure with identical unit cell dimensions of alternating tetrahedral and octahedral layers (Bragg, 1915). In the crystal structure, Fe^{2+} ions and half of the Fe^{3+} ions occupy octahedral sites whereas the other half of Fe^{3+} ions occupy the tetrahedral site**.** The magnetic moment of trivalent iron ions in octahedral sites is equal but opposite to the magnetic moment of divalent iron ions in the tetrahedral sites. So, the net magnetic moment in magnetite is given by Fe^{+2} ions in the octahedral sites. Each unit cell consists of 32 oxygen atoms, 16 Fe^{3+} ions and 8 Fe^{2+} ions in a face centred cubic structure (Kozlovskiy et al., 2019).

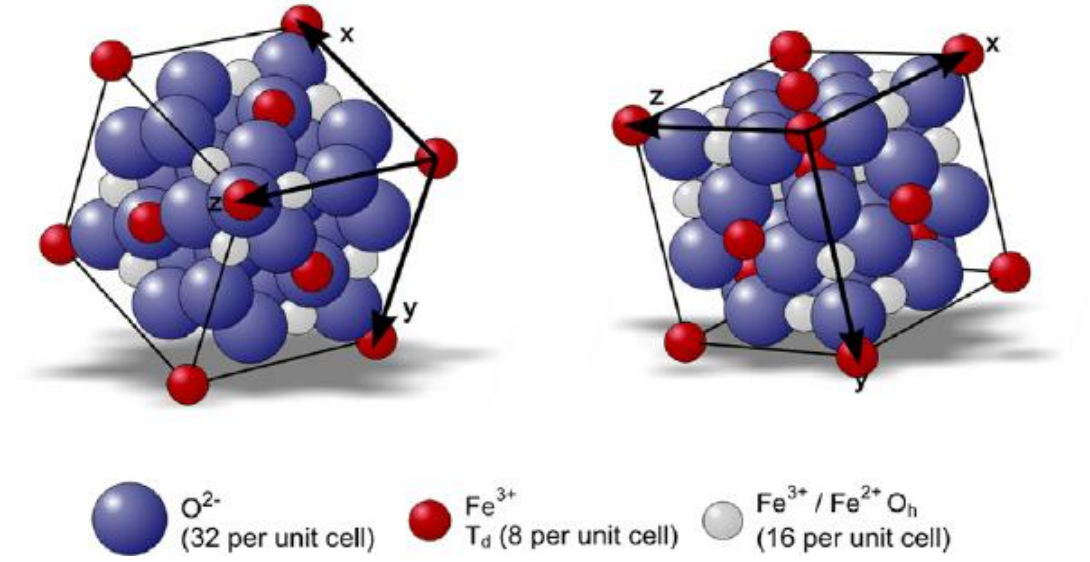

Figure 1.3: Unit cell of magnetite crystal (Schmitz-Antoniak, 2015)

Figure 1.3 shows the unit cell of magnetite crystal. Here, each particle in blue colour and with large size represents O^{2-} ion. Similarly, smaller size particles in red colour represent Fe^{3+} ions in tetrahedral sites and particles in white colour represent Fe^{3+} and Fe^{+2} ions in octahedral sites. The axial length and interfacial angle for a unit cell are a=b=c= 0.839 nm and $\alpha=\beta=\gamma= 90^{\circ}$.

Biologically, magnetite particles are found in different organisms from bacteria such as *Magnetospirillum magnetotactium*, to higher animals including human beings. It is found in the hippocampus of the organism and is involved in information transfer, memory and learning. Magnetite is also found in the brain of bees as well as birds which allows them to sense the direction of the earth's magnetic field. Molluscs such as snails have magnetite teeth as well as the tongue that makes it abrasive to help them grab food from rocks (Frankel & Blakemore, 1989).

Several chemical methods can be used for the synthesis of magnetite NPs such as sol-gel (Hamed Sadabadi, 2015; Hu et al., 2019; Takai et al., 2019; Xu et al., 2007), microemulsion (Liang et al., 2010; Salvador et al., 2021; Singh & Upadhyay, 2018), solvothermal (Tian et al., 2011; B. Sen Yadav et al., 2020), sonochemical reduction (Andrade et al., 2012; Cheng et al., 2005; V. K. Yadav et al., 2020), hydrothermal (Torres-Gómez et al., 2019), coprecipitation (Nkurikiyimfura et al., 2020), hydrolysis and thermolysis of precursors, flow injection, electron spray and pyrolysis. Each of all these methods has its own advantages as well as difficulties.

Due to their unique properties, magnetite nanoparticles have been widely used in several fields. The promising applications of such size-controlled materials have been found in magnetic recording media such as audio and videotape, catalysis, adsorption of heavy metals, biomedical uses including in drug delivery systems, radiofrequency hyperthermia, magnetic resonance imaging (MRI), cancer therapy, and many more (Fato et al., 2019; Karami, 2013; Linh et al., 2018; Maity et al., 2010; Prilepskii et al., 2018; Schwaminger et al., 2017).

1.4 Objectives

The broad objective of this study is to synthesize magnetite nanoparticles (MNPs) of controlled size via microemulsion technique using edible oil as oil phase. The specific objectives of the study include:

1. Synthesis of MNPs using microemulsion technique with hexane, mustard oil and soybean oil as oil phase, and
2. Study of the effect of different oil phases on morphology, size as well as band gap energy of the prepared MNP_s.

CHAPTER 2
LITERATURE SURVEY

2.1 Unique Properties of Nanostructured Materials

Nanoscale materials can have quite different properties as compared to their bulk analogues. As the size of the particle approaches the nanoscopic range, some of the properties such as hardness, strength, ductility, elastic modulus, melting point, density and thermal conductivity of the material change significantly (Kozlovskiy et al., 2019; Murty et al., 2013; Radoń et al., 2017; Salvador et al., 2021; Yoshida & Lahann, 2008). For instance, differences in some of the major properties of nickel (Ni) in its nanoscopic range as compared to its microscopic range are shown in Table 2.1.

Table 2.1: Comparison of properties of nickel (Ni) in microscopic and nanoscopic range (Murty et al., 2013)

Properties	**Change in property**
Hardness	Increases by 5 times
Strength	Increases by 3-10 times
Corrosion resistance	Reduced (localized corrosion)
Electrical	Resistivity increases
Wear Resistance	Increases by 170 times
Frictional coefficient	Reduce to half
Saturation magnetization	Reduce by 5 %
Electrocatalytic property	Enhance the evolution of hydrogen

Particles at the atomic level show completely different properties as compared to bulk. So, properties such as melting point, mechanical strength, optical, microbial properties, exciton, magnetic domains, super hydrophobicity of the NPs always depend upon the size of the particle. These different properties are mainly due to their high surface to volume ratio. Due to these unique properties of the particle at the atomic level, nanomaterials include a wide range of applications in physics, chemistry, material science, optics, biomedical science (Boufas et al., 2020; Ghimire et al., 2016; Horst et al., 2017; Kozlovskiy et al., 2019; Rashid et al., 2017).

Some unique properties of nanomaterials are discussed below:

2.1.1 Antimicrobial properties:

Nanomaterials show different properties to microorganisms as compared to bulk material. Non-metallic, metallic, as well as metal oxide nanoparticles, are mostly used in the biomedical field for cell treatment. The antimicrobial properties of the nanomaterial proceed either through the physical or chemical mechanism. For CNTs, the physical mechanism is due to the structural damage of the cell wall and membrane of the microorganisms. The structure of the nanomaterial is responsible for such phenomena. Some chemical interactions between the nanomaterial and cell can cause oxidative stress and ultimately can cause the death of the cell. Some mechanisms also include the electron transfer between the cell and nanomaterial (Al-Jumaili et al., 2017).

Metallic nanoparticles such as gold, silver, magnesium etc. have been widely studied as antimicrobial agents due to their low toxicity. Not only the metallic form but also metal oxide had been studied and proven as the material to kill bacteria, viruses as well as fungi through cell membrane damage and the formation of reactive oxygen species as shown in Figure 2.1 (Gharpure et al., 2019).

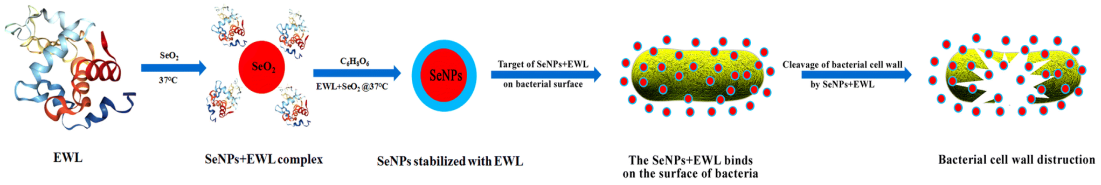

Figure 2.1: Antimicrobial mechanism of SeO_2 nanoparticle (Muthu et al., 2019)

2.1.2 Quantum confinement:

Optical, electronic, magnetic property difference is due to the quantum confinement effect. The quantum confinement effect arises when the size of the particle is too small as compared to the wavelength of the electron. Here, the term quantum represents the atomic realm of particles and confinement means to confine the motion of randomly moving electrons to restrict motion in specific energy levels. The confinement of the electrons and holes always depends on the properties of material called Bohr's radius (Dorfs et al., 2019).

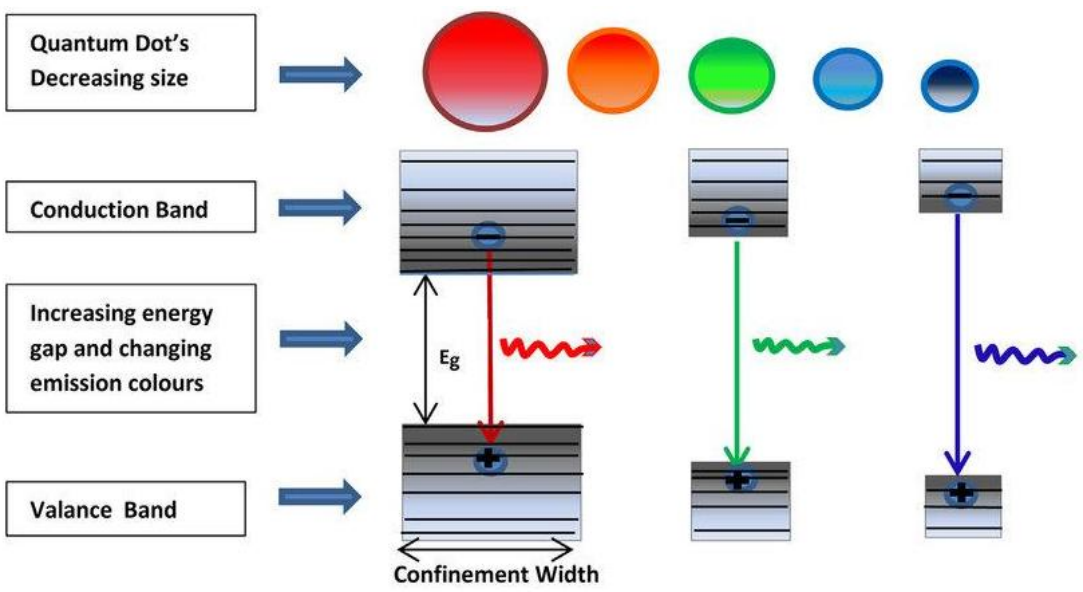

Figure 2.2: Change in optical property due to quantum confinement effect (Jagtap et al., 2019)

2.1.3 Surface plasmon resonance (SPR):

The measurement of tiny molecules in the very dilute concentration of analyte plays a crucial role in a variety of fields, from the food industry to biological, pharmacological, and therapeutic applications. Based on their interaction with biomolecules, these small molecules can be suitably detected by surface plasmon resonance. The formation of surface plasmons will be at the interface of two materials, one of the interfaces is a metal with a lot of free conduction electrons and the other is a dielectric. Surface plasmon resonance is not only limited to the multimolecular layer but is also more evident for metal particles with dimensions that are much smaller than the wavelength of interacting light. However, the system's sensitivity for detecting these compounds is quite poor. For years, improving sensitivity has been a struggle and many strategies have been tried to improve SPR signals. The use of a variety of nanomaterials to improve SPR signals has yielded promising results. In addition to this benefit of employing nanomaterials, signal amplification afforded by the proper use of reflected light phase information could be useful in improving SPR sensitivity. Traditional SPR sensors are unable to detect tiny changes in the target's exterior qualities, however, phase-sensitive SPR sensors can (Li & Zhang, 2017).

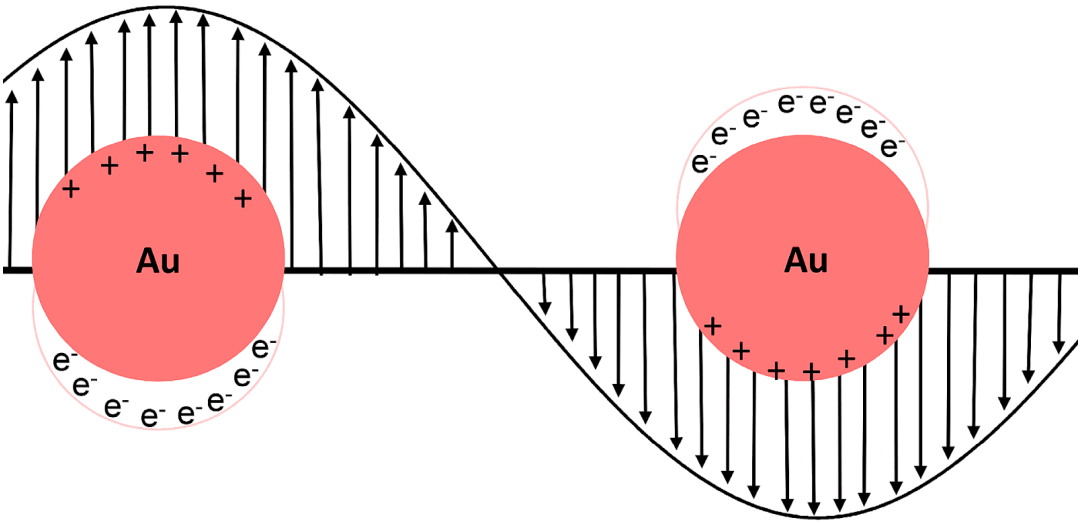

Figure 2.3: Surface plasmon resonance of gold nanoparticle (Szunerits et al., 2014)

2.2 Iron Oxide Nanoparticles and Their Properties

2.2.1 Various forms of iron oxides

The magnetic properties of any material depend upon its size, shape, structure, crystallinity, synthetic method as well as nature of metal. The magnetic properties over a magnetic field whenever is weak have no significant effect on the living organism. However, the use of high strength field can have a significant impact. Recently, a large number of works had been carried out to study and use these magnetic NPs in the adsorption of heavy metal ions from waste water as well as magnetic field hyperthermia (Horst et al., 2017).

One of the most abundant metals on the earth's surface is iron and it is found in the form of oxide. Iron oxide has oxidative stability, compatibility in the non-aqueous system, and nontoxicity. Yellow iron has been used as the pigment for several years in catalysts, jewellers, adsorbents, batteries, electrodes, medicines, fertilizers and raw materials for the iron and steel industries. According to Cornell and Schwartzman there are 17 types of iron oxides ranging from oxides, hydroxides and oxihydroxides (Boufas et al., 2020; Zeng et al., 2016).

Oxide, hydroxide and oxyhydroxide crystal of iron can be ferromagnetic, antiferromagnetic and ferrimagnetic as Fe^{2+} ion contains four unpaired electrons in 3d

shell and Fe^{3+} ion contains three unpaired electrons in 3d shell. Out of all the oxide ores of iron, magnetite (Fe_3O_4) and Maghemite (Γ-Fe_2O_3) are mostly used to make superparamagnetic materials (Zeng et al., 2016). Table 2.2 shows different oxides, hydroxides and oxyhydroxides of iron with their molecular formula and local name.

Table 2.2: Classification of natural iron oxides, their molecular formula and minerals names

Type of compound	Molecular formulae	Name of the compound
Oxide	α-Fe_2O_3	Hematite
	Fe_3O_4	Magnetite
	Γ-Fe_2O_3	Maghemite
	β -Fe_2O_3	
	ε -Fe_2O_3	
	FeO	Wustite
Oxide- Hydroxide	α –FeOOH	Goethite
	Γ –FeOOH	Lepidocrocite
	β –FeOOH	Akagetite
	$Fe_{16}O_{16}(OH)_y(SO_4)_z.nH_2O$	Schwertmannite
	δ- FeOOH	
	δ '-FeOOH	Feroxyhyte
	FeOOH	
Hydroxides	$Fe_5HO_8.4H_2O$	Ferrihydrite
	$Fe(OH)_3$	Bernalite
	$Fe(OH)_2$	
	$Fe_x^{iii}Fe_y^{ii}(OH)_{3x+2y-z}(A^-)_z$	Green rust

There are different forms of iron oxides in nature. The most common iron oxides that are important in scientific technology are magnetite, maghemite, and hematite. Other oxyhydroxides and hydroxides consist of minerals bearing oxygen. As per the review, the (OH^-) group of the hydroxides forms structures resulting in lower bond strengths than the oxide minerals.

2.2.2 Methods for producing nanoparticles

Magnetic properties of nanomaterials are powerful manipulation and detection tools which have been studied for a long time. Magnetic nanoparticle acts as the active component of ferro fluids, recording tape, flexible disk recording media, as well as biomedical materials and catalysts. Assembly of magnetic grains also has been used

in hard disk recording media, permanent magnets, and nanocrystalline soft materials (Kodama, 1999).

In the last few decades, significant progress has been made in the synthesis of nanoparticles. Based on the approach, methods for nanoparticle synthesis can be divided into the following two ways: (Choi et al., 2008; Saleh, 2020)

I. **"Bulk to nano" approach:** This method consists of breaking down the bulk material into nanoparticle size. In the approach, a bulk material in its solid form is taken as starting substrate. Such material is then processed through either wet or dry methods for reduction of its size. A large quantity of the particle can be synthesized within a short period by this method. This method is commonly called as a top-down approach.

II. **"Atom to nano" approach:** This approach includes the synthesis of nanoparticles from the atomic level. The liquid, as well as gas phase of the material, is taken as starting material for such an approach. This approach is also known as the bottom-up approach. As compared to the top-down approach, the bottom-up approach has a high tendency to obtain shape and size-controlled nanoparticles. Table 2.3 shows some of the nanoparticles synthesized from these approaches.

Table 2.3: Different methods for nanoparticle synthesis (Ealias & Saravanakumar, 2017)

Approaches	Methods	Examples of nanoparticles synthesized
Atom to Nano	Sol-gel	Carbon, metal and metal oxide-based materials
	Spinning	Organic polymers
	CVD	Carbon and metal-based materials
	Pyrolysis	Carbon and metal oxide-based materials
	Biosynthesis	Organic polymers and metal-based materials
Bulk to Nano	Mechanical milling	Metal, oxide and polymer-based materials
	Nanolithography	Metal based materials
	Laser ablation	Carbon based and metal oxide based materials
	Sputtering	Metal based materials
	Thermal decomposition	Carbon and metal oxide based materials

Among various solution mediated techniques, sol-gel and micro-emulsion methods frequently seem for nanoparticle synthesis are discussed in the following paragraphs.

Sol-gel method: Sol-gel technique is one of the most promising techniques for the preparation of both pure solid as well as composite based nanomaterials. Molecular scale homogeneity, low proceeding temperature and the possibility of incorporation of many different metal dopants in the different matrices are some advantages of this technique. This procedure consists of a diphasic system, solid phase and liquid phase where sol is formed which then slowly proceeds towards a gel-like structure. Typical precursors of the sol-gel technique are metal alkoxide and metal chlorides, which undergo both polycondensation and hydrolysis to form a colloidal particle. The size of the forming particle is then varied from the colloidal size to the solid phase matrix size (Hamed Sadabadi, 2015; Sara shaker, Shirzad Zafarian, Shilpa chakra, 2013; Xu et al., 2007). Example of nanoparticles synthesized by the sol-gel method is titanium oxide (TiO_2), zinc oxide (ZnO), aluminium oxide (Al_2O_3), iron oxide (Fe_2O_3, Fe_3O_4) (Habte et al., 2019; Irshad et al., 2018; Tabesh et al., 2018; Tadic et al., 2019).

In the sol-gel technique, the solution of salt precursors is initially hydrolyzed followed by condensation to form a colloidal suspension called sol. During condensation, water or alcohol is removed to form the metal oxide or hydroxide linkage. Sol is then converted to viscous gel and solid material as shown in Figure 2.4. The gel is finally dried for evaporation of the solvent and ground to obtain powder nanoparticles (Murty et al., 2013).

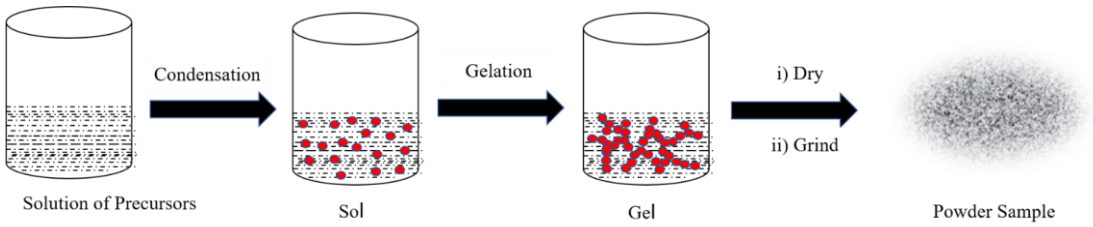

Figure 2.4: Sol-gel technique for nanoparticle synthesis

Microemulsion method: The microemulsion method was used first by Schulman by preparing a quaternary solution of water, benzene, hexanol and potassium-olate. Generally, oil and water are immiscible in the normal condition, so they separate into two phases when mixed with an interfacial tension of about (30 dynes/cm - 50

dynes/cm) (Eastoe et al., 2006). This can be overcome by the use of surface-active reagents commonly called surfactants. Surfactant contains hydrophilic as well as lipophilic properties. If a suitable amount of surfactant is used, it creates an interface between the water and oil phase decreasing the interfacial tension. Similarly, a cosurfactant is also used to increase the stability of microemulsion. It is found that this system consists of particles having a diameter between 600 nm and 800 nm (Kumar & Mittal, 1999).

Reverse microemulsion or water dispersed in oil (w/o) is thermodynamically stable isotropic dispersion of water in the continuous oil phase. These two phases are also stabilized by the use of proper surfactant molecules. The oil phase of such a system is generally compound having a chain of 5 to 12 carbons. In many cases, alcoholic compounds such as isopropyl alcohol have been used as co-surfactant. The use of the co-surfactant in the reaction system further increases the stability of the emulsion. An emulsion is formed via agitation of oil and water. It results in two-phase dispersion droplets being coated with the surfactant. This surfactant is determined based on the phase. The use of hydrophilic surfactant compels the emulsification of oil in droplets throughout a continuous aqueous phase. On the other hand, the water is emulsified in droplets dispersing continuously in the oil phase when a lipophilic surfactant is used (Al-Jumaili et al., 2017; Malik et al., 2012).

Synthesis of NPs through microemulsion can be carried out by using two solutions, one consisting of salt precursor and another with a reducing agent. When these two solutions are mixed collision between two nanodroplets occurs which is called percolation.

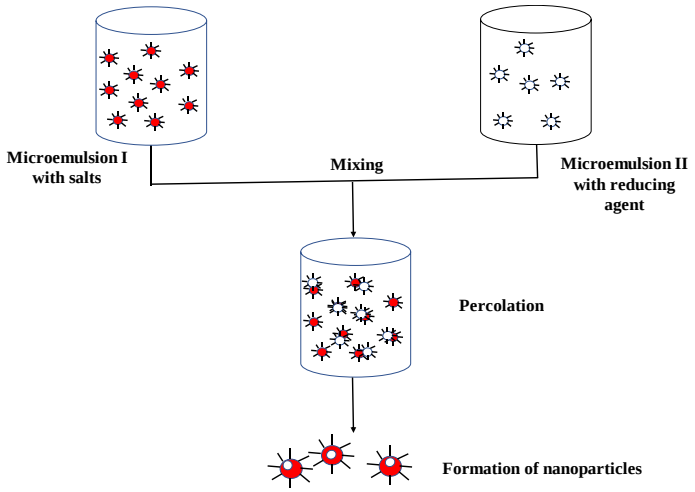

Figure 2.5: Microemulsion technique for nanoparticle synthesis

Due to these advantages, several metallic, as well as non-metallic nanoparticles, have been successfully synthesized by this method. This method is mostly applicable in the fields of biology and chemistry with the ability to control particle properties (Ghimire et al., 2016).

Nanoparticles can also be prepared using these methods. A comparison between different methods with their advantages and disadvantages is shown in Table 2.4.

Table 2.4: Comparison of different methods for the fabrication of NPs

Method of preparation	Advantages	Disadvantages	References
Coprecipitation	synthesize large amount of water soluble and biocompatible NPs	low control of particle shape broad distribution of size and aggregation of particles and uncontrolled oxidation.	(Ahn et al., 2012; Ma? et al., 2014)
Sol gel	control of morphology and chemical composition desired shape and length	expensive alkoxide reactants, need high temperature for calcinations time consuming	(Hamed Sadabadi, 2015; Xu et al., 2007)
Hydrothermal	smaller size and lower crystallinity	affect the properties of particles by the molar ratio of salt.	(Daou et al., 2006; Khollam et al., 2002)
Microemulsion	uniform properties and size of the NPs	difficult to remove surfactant low synthesis	(Liang et al., 2010)
Aerosol/vapor (pyrolysis)	high production rate	large aggregates	(Lyubutin et al., 2019)

Several techniques have been used for the synthesis of magnetite nanoparticles. Some of the methods adapted and properties of MNP_s is given in Table 2.5.

Table 2.5: Different approaches for MNPs synthesis

Method of synthesis	Reagents	Properties of particles	References
Microemulsion technique	0.3M $FeSO_4$ and $Fe(NO_3)_3$ in the aqueous phase, cyclohexane as oil phase and NP5+NP9 as the surfactants	Size: <10nm	(Zhou et al., 2001)
Coprecipitation method	ferrous and ferric ions by NaOH in an aqueous solution.	Particle Size: 3 to 20 nm Disadvantage: adjustment of pH, < 20 nm	(Sun & Zeng, 2002)
Microwave hydrothermal method	ferrous sulphate and sodium hydroxide	Size: 0.15-0.2 nm.	(Khollam et al., 2002)
Microemulsion technique	$FeCl_3$ and $FeCl_2$, NaOH. sodium dodecyle benzene sulfonate (DBS), ethanol	Size: 10 nm	Liu et al., 2004
Co-precipitate followed by hydrothermal	$[N(CH_3)_4OH]$ solution	Size: 12 nm	(Daou et al., 2006)
Thermal decomposition	acetyl-acetonate, iron carbonyl and iron cupferronates, oleylamine, oleic acid, steric acid	Size: 2 to 30 nm	(Majewski & Thierry, 2007)
Microemulsion technique	n-heptane, n-hexanol	Size: < 16 nm	Lu et al., 2013
Microemulsion technique	oleic acid, isopropyl myristate (IPM), brij-97, transcutol, polyethylene glycol 400 and propylene glycol		Daik et al. 2017

Magnetite has been prepared by various methods with a wide range of possible applications. However, the toxicity of the nanomaterials, different rate of deposition

of ferrous and ferric ions, irreproducibility of the synthetic method and separation in its pure form after application are some challenges during magnetite synthesis. Interchange in the crystal structure and instability of the prepared materials over a long time due to agglomeration is also an issue (Sharifi et al., 2012). This work would be focused in the size-controlled synthesis of MNPs taking these all limitations into account.

2.2.3 Applications of magnetite nanoparticles

I. Magnetite nanoparticles in heavy metal removal

Environmental pollution is currently one of the major problems faced by living organisms. With the increase in the population, nature, as well as natural resources, has been consistently affected by different actions carried out by human beings. The contamination of the water with heavy metals' ions such as copper, iron, lead, chromium etc. has exceeded. If such metals exceed their permissible limit they can cause both short and long term harmful effects which will make the survival of living organisms harder in the next few years. Waste water produced by different industries such as mining, alloy, Chlor-alkali, radiator manufacturing, battery manufacturing as well as electroplating is playing a leading role to cause the increase in the concentration of these metals ions in natural resources (Yunus et al., 2020). These metals do not degrade easily and their accumulation in the living organism can cause several health problems such as renal failure, oral ulcer, cancer, kidney failure, metabolic acidosis etc (Shen et al., 2019). Excess of these elements which are necessary in trace quantity for metabolic function in biological system, results in higher degree of problems in the aquatic system also. So, the removal of these metal ions from the waste water is important (Trivedi et al., 2007).

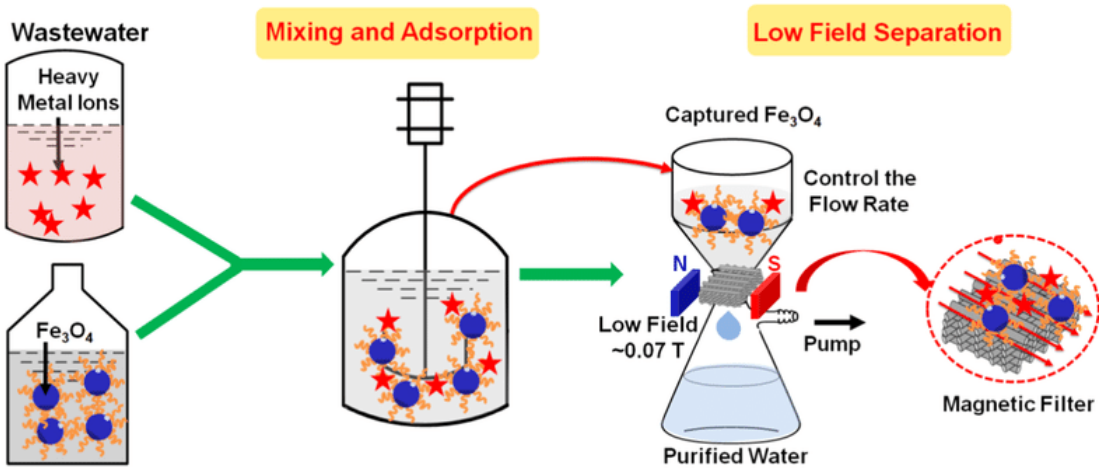

Figure 2.6: Illustration of a magnetic adsorption process (Wei et al., 2017)

Amine-functionalized mesoporous Fe_3O_4 nanoparticles (AF-Fe_3O_4) had already been developed and used for the highly efficient removal of toxic heavy metal ions from water. The maximum amino group grafted onto AF- Fe_3O_4 was 0.1790 μg/mg as identified by the ninhydrin test. AF- Fe_3O_4 was also simply recovered from the water with magnetic separations at a low magnetic field within 1 min. Thermodynamic studies showed that the adsorption process was endothermic and spontaneous. The maximum removal was over 98% of Cu(II), Cd(II) and Pb(II) in 50 mL of a solution containing 5 mg/L metal ions (Xin et al., 2012).

The advantage of the magnetite nanoparticle over classical adsorbents on removal of the heavy metals ions from the solution is due to their high adsorption capacity. The high surface to the volume ratio in nanomaterial leads for effective removal of such metal ions. High dispersion of the material during water treatment and their paramagnetic behavior makes them as nobel adsorbent. Separation of the metals loaded over such type of adsorbent can be easily carried out using an external field and also the adsorbent can be reused (Giraldo et al., 2013).

II. Magnetite nanoparticles in biomedical application

Magnetite nanoparticles had been widely used for bioanalytical and biomedical applications such as in biosensors, bioimaging, targeted drug delivery and signal markers. Among magnetic nanoparticles of nickel, cobalt and iron, magnetite nanoparticle is mostly used due to their low toxicity and high oxidation stability. However, for the application of MNPs in the biomedical field, size of the particle

must be less than 20 nm. Below this size, they exhibit the superparamagnetic property that is required for biomedical applications such as magnetic imaging. However, the agglomeration of the particle to reduce the surface energy and magnetism loss due to oxidation limits their application. Encapsulation of MNPs by organic polymer and inorganic material helps to increase stability as well as bioconjugation.

Most two most common applications of MNPs in the biomedical field are targeted drug delivery and magnetic fluid hyperthermia. Folic acid-coated magnetite nanoparticle of size 3 nm to 13 nm was successfully prepared by using the precipitation method. The nanoparticle thus formed was then loaded with curcumin. Cyclodextrin cavities were saturated between 0.3 mg to 0.5 mg of curcumin with the release of the drug up to 80 % within a short period (Salem et al., 2015). Similarly, the core/cell nanoparticle of Fe_3O_4/ SiO_2 encapsulated with PEG-PLA was prepared by using the precipitation polymerization process. Such microsphere showed low toxicity even at high concentrations with high loading efficiency of nearly 50 % (Deng & Lei, 2013).

In magnetic fluid hyperthermia, heat is used to kill tumours cell inside the body. The source of heat is the magnetic nanoparticle which can generate heat through the hysteresis loss in the presence of the external magnetic field. As temperature increases up to 45℃, local cell death occurs due to apoptosis as well as necrosis (Estelrich & Antònia Busquets, 2018).

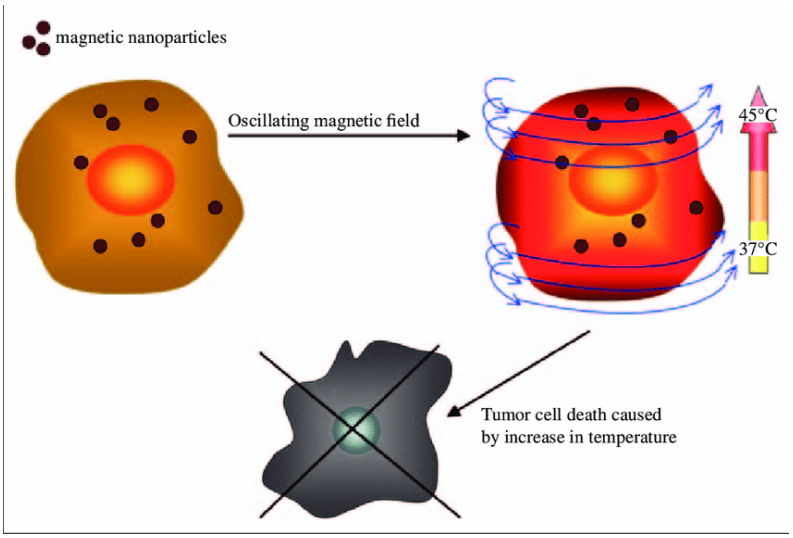

Figure 2.7: Illustration of a typical magnetic hyperthermia therapy process (Latorre & Rinaldi, 2009)

III. Magnetite nanoparticles in electrical application

Most of the iron oxide falls in the category of semiconductor where the energy gap between the valence band and conduction band is less than 5eV. For the excitation of an electron from valence or to the conduction band, external energy such as visible light of appropriate energy is needed. Among all the semiconductors with partially filled lattice band, MNPs shows abnormally good conductor. At room temperature, it shows the resistivity in the range $10^{\wedge -4}$ to $10^{\wedge 9}$ Ωm which is significantly higher i.e. $10^{\wedge 6}$ times greater than Fe_2O_3 and that is due to the exchange of electrons in the Fe^{+2} and Fe^{+3} centres. The electrons coordinated with these iron species within the magnetite structure. Due to electron delocalization effects, magnetite can be slightly deficient on octahedral sites. Such deficiency allows for n-type and p-type magnetite semiconductors (Boufas et al., 2020; Weidenfeller et al., 2002).

CHAPTER 3

EXPERIMENTAL

3.1 Materials

Ferric chloride anhydrous (99%, Fisher Scientific, India) and ferrous sulphate heptahydrate (98%, Fisher Scientific, India) were used as salt sources. Ammonia (25%, Fisher Scientific, India) was used as the precipitating agent for the synthesis of MNPs. Hexane (Glaxo Laboratories, India), commercially available edible mustard oil and soybean oil were used as the oil phase in the microemulsion. Sodium dodecyl sulphate (SDS) (Fisher Scientific, India) was used as the surfactant whereas isopropyl alcohol (Glaxo Laboratories, India) as a cosurfactant. All reagents were of laboratory grade and used without further purification. Distilled water was used in all the experiments if required.

3.2 Preparation of Solutions

3.2.1 Preparation of microemulsions

Three different microemulsions were prepared with an identical water/oil (w/o) ratio of 1:10 (v/v) using hexane, mustard oil and soybean oil as different oil phases using a standard protocol.

In a typical experiment, 46 mL of each oil phase (hexane, mustard oil and soybean oil) was mixed with 2.6 mL of water, 0.8 gm of surfactant and 13.4 mL of cosurfactant in a 250 mL conical flask. The mixture placed in the thermostat at 40 ℃ was homogenized with the help of a magnetic stirrer for 30 minutes until a clear microemulsion was obtained. The formation of microemulsion was attested by the transformation of the opaque heterogenous mixture to a homogenous solution due to the formation of the possible nanoscale microemulsion. (See Figure 3.1)

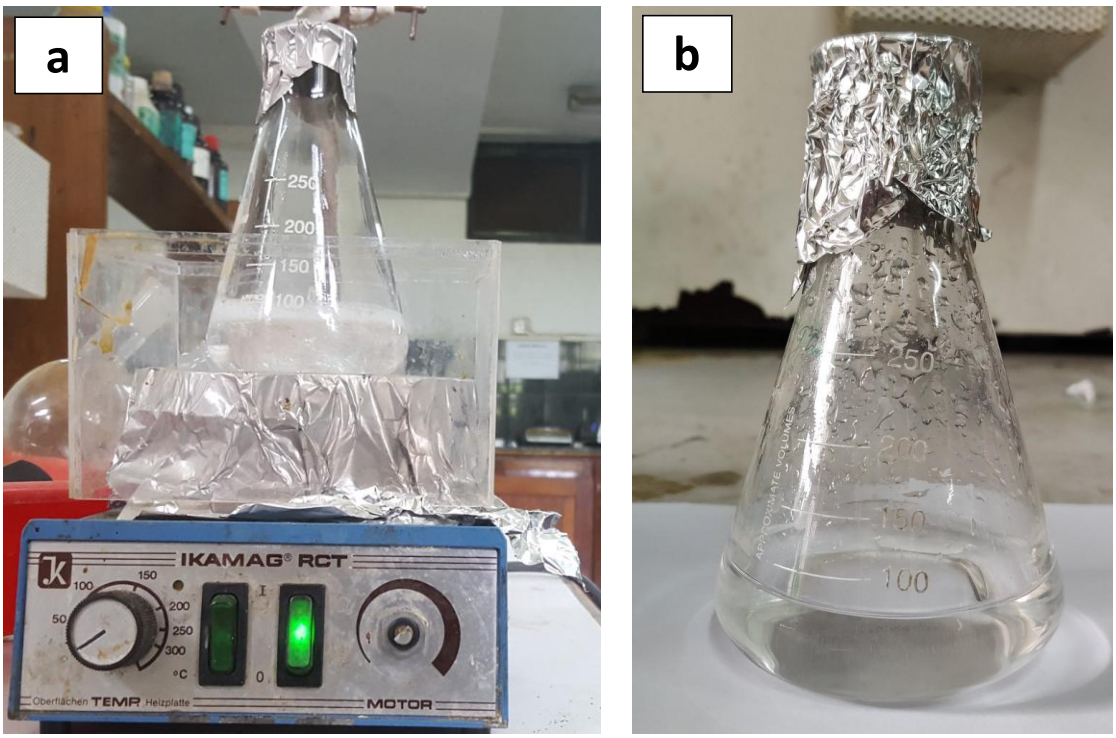

Figure 3.1: Photographs showing the change in solution transparency due to microemulsion formation: a) translucent solution before, and b) transparent solution after the stirring for 30 min

Each of the microemulsions was divided into two equal volumes and named ME (I) and ME (II).

3.2.2 Preparation of microemulsion containing the salt precursor:

To the ME (I) of each type, 2.7 gm of $FeSO_4$ (0.1 mol) was added and stirred to completely dissolve the salt. Then 0.81 gm of $FeCl_3$ (0.05 mol) was added (at a molar ratio 2:1 of salts) to the resulting solution with constant stirring. The mixture was stirred for 30 minutes under an argon gas atmosphere at 40 ℃.

3.2.3 Preparation of microemulsion containing the precipitating agent:

To the ME (II) of each type, 7.5 mL of ammonia was added and stirred for 30 minutes.

All the solutions were stored safely in the lab at 25 ℃.

3.3 Preparation of Magnetite Nanoparticles (MNPs):

Each microemulsion containing ammonia ME (II) was poured dropwise into the microemulsion containing the precursor salts solution ME (I). The color of the mixture immediately changed to black. The mixture was stirred for two hours using a magnetic stirrer.

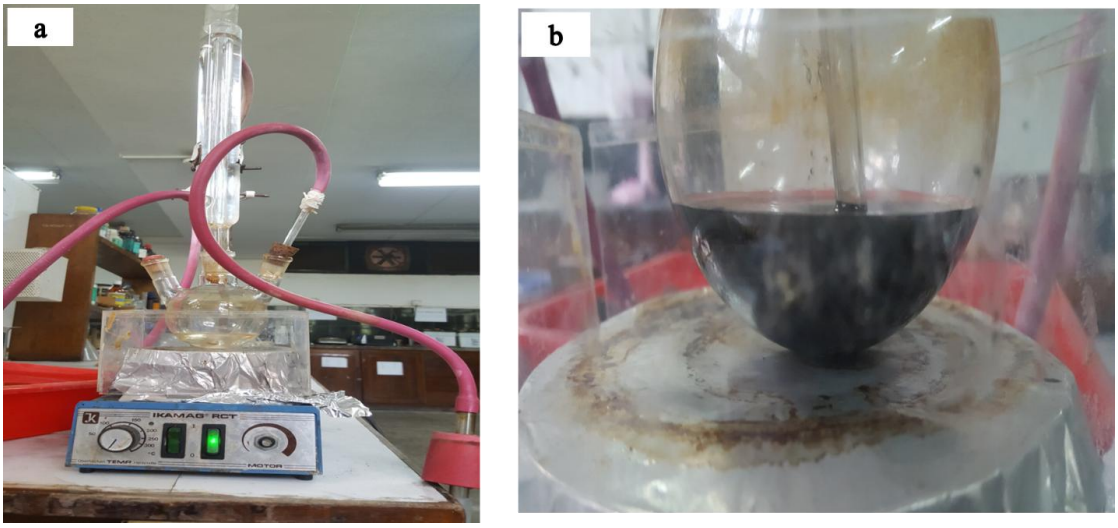

Figure 3.2: Photographs showing the preparation of MNP_s: a) the apparatus showing the arrangement of the inert gas environment during synthesis, and b) MNPs containing a round-bottom flask showing black precipitate

Black-colored particles were then separated using a bar magnet. A bar magnet was made close to the particle and the solution was discarded. The sample was then washed with an ethanol-water mixture at a volume ratio of 1:1. For this, ethanol-water was added to the sample, sonicated for 5 minutes and centrifuged. The process was repeated 3 times. The sample was dried in a muffle furnace at 100 ℃ under an argon gas atmosphere for an hour. The dried sample was then kept in a sealed vial for further characterization.

The procedure for the synthesis of MNPs using microemulsion is presented in Scheme 3.1.

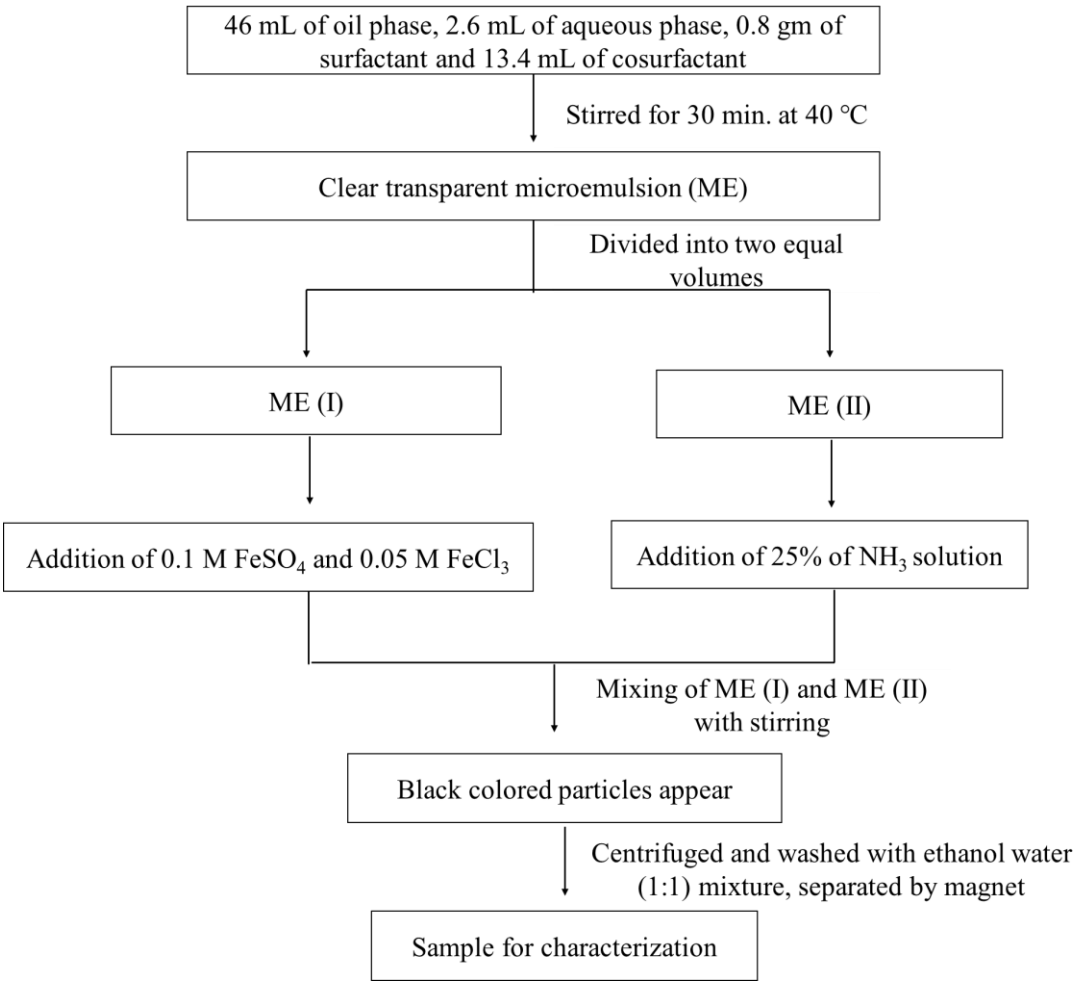

Scheme 3.1: Procedure for the synthesis of MNPs using microemulsion technique (Satter et al., 2014)

3.4 Characterization Methods

3.4.1 Preliminary characterization

The freshly prepared powder of the magnetite was taken on a clean dry white sheet of paper and a magnetic fish was brought close to the sheet to observe the response of the powder sample to the external magnetic field; shown in Figure 3.3a.

To further characterize the magnetite powder, 0.1 g of the powder was dispersed through ultrasonication in the ethanol and water mixture (volume ratio of 1:1) in a 15 mL glass vial. The dispersed solution was then studied through a laser beam to observe the light scattering property, the Tyndall effect; shown in Figure 3.3b.

Morphology and particle size determination was also done using Boeco BM-800 binocular microscope with B-CAM 16 digital camera. The sample was finely ground and was spread onto the glass slide and observed under the optical light.

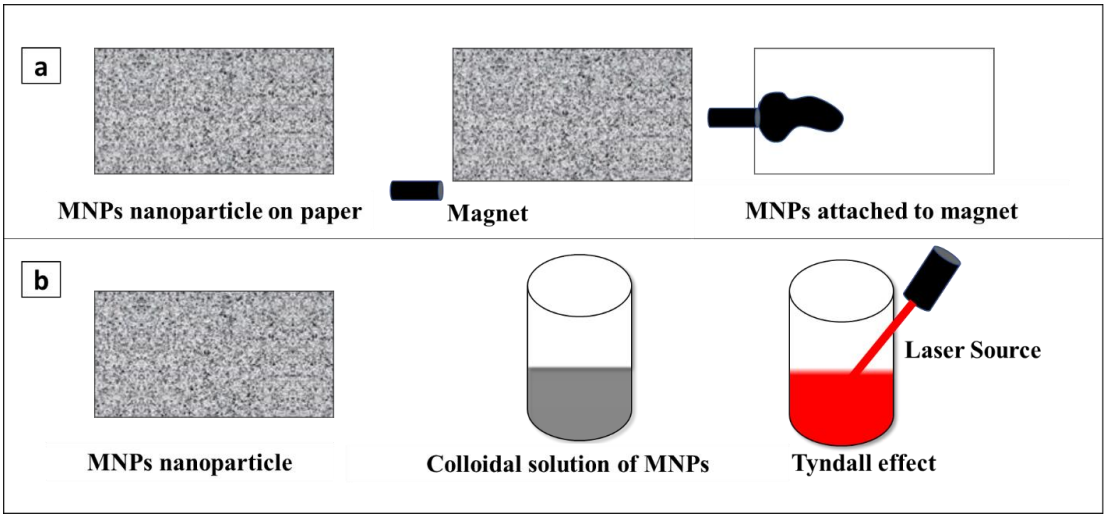

Figure 3.3: Illustration for preliminary study of physical properties of synthesized powder: a) magnetic property, and b) Tyndall effect

3.4.2 X-Ray powder diffraction (XRD)

The crystal phase and structure of the samples were investigated by an X-ray diffractometer (Bruker D2 Phaser) equipped with CuKα radiation, λ = 0.15418 nm and the pattern were recorded at a scanning rate of 0.1˚/step and 2θ angle ranging from 20° to 80°. The acceleration voltage of 35 kV and emission current of 30 mA were used.

The obtained patterns were baseline corrected using the ALS system and then smoothed to 15 points (Savitzky-Golay) using Originpro 2016 (64 bits).

3.4.3 Fourier transform infrared (FTIR) spectroscopy

The FTIR spectra were recorded using IR Affinity-1 FTIR Spectrometer (Shimadzu) to identify species, functional groups, and vibration modes associated with each peak. Spectra were collected in the spectral range of 4000–400 cm^{-1} with a spectral resolution of 4 cm^{-1}.

3.4.4 Ultraviolet-visible (UV-Vis) spectroscopy

For the UV-Vis analysis, the colloidal solutions of samples were prepared in the ethanol-water mixture (1:1 volume ratio) with multiple ultrasonication. Absorbances were studied through a UV spectrophotometer (Shimadzu UV-1900i, Japan) using a 10 mm quartz cuvette. Deuterium lamp and halogen lamp of 20 W were used as the source for UV and visible lights respectively. Silicon diode was used as the detector to obtain the spectra. Lights of wavelengths 190 nm to 800 nm were used for the study of absorbances characteristics of the MNPs.

To obtain the corresponding direct transition band gap energy of particles, tauc plot was done. The method for the determination of band gap energy is based on the following equation. (1).

$$(\alpha h\nu)^2 = B\,(h\nu - E_g) \quad \ldots\ldots\ldots\ldots\ldots\ldots \quad (1)$$

Here, ν represent the photon's frequency, h the Planks's constant and α the absorption coefficient, B a constant and E_g the band gap energy. (Makuła et al., 2018)

Surface plasmon absorbances and tauc plots were sketched using OriginPro 2016 (64 bit).

3.4.5 Scanning electron microscopy (SEM)

SEM was performed using an FEI Quanta 650 ESEM-FEG operated at 15 kV. For SEM analysis, sample powders were dispersed in distilled water by ultrasonication (Hielscher ultrasonic processor UP500S, 400 W, 24 kHz, tapered tip probe), with 65% amplitude for 3 min in the pulse mode (0.5 s pulse/pause). Dispersions were then pipetted on a glass slide. After drying at 60 °C on a hot stage, the glass slide with the dry powder was carbon coated for electrical conductivity (10 nm C-layer).

The average size of particles obtained from each method was measured by Image J software. At least 20 particles were selected to calculate the average diameter of the particles, and further normal distribution curves were fitted using OriginPro 2016 (64 bit).

CHAPTER 4

RESULTS AND DISCUSSION

4.1 Preliminary Characterization

The results from preliminary characterization can deliver information such as color, magnetic property as well as light scattering properties of the particles.

Figure 4.1 shows a powdery texture (Figure 4.1a) and the magnetic nature of the sample in the presence of an external bar magnet (Figure 4.1b). It can be observed that powder samples were black-colored identical to the color of MNPs as given in the literature (Niculescu et al., 2021). All powder samples were attracted to the magnet demonstrating the magnetic nature of the particles.

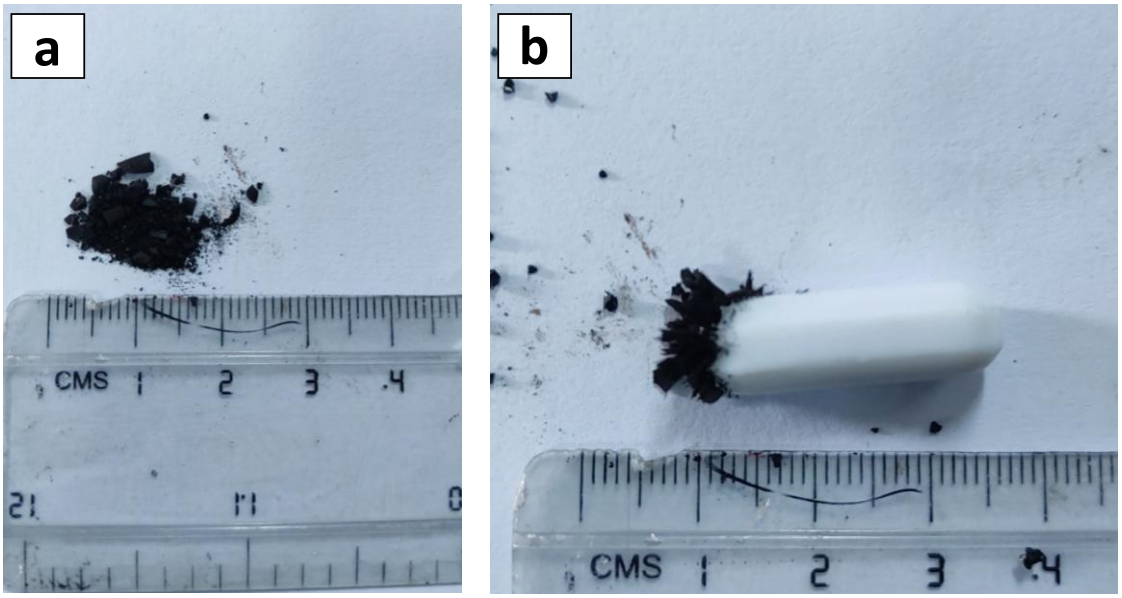

Figure 4.1: Photographs showing MNPs: a) physical appearance of MNPs, and b) magnetic nature of particles shown by their attraction to magnetic fish

Figure 4.2 shows the photograph of the response of the colloidal solution of the particle towards laser light (Figure 4.2a) and an optical micrograph of the particles (Figure 4.2b). The scattering of the laser light can be seen, as a basic property of the colloidal solution in which particles have dimensions comparable to that of visible light (nanometer scale). The scattering of light through the colloidal solution is called Tyndall effect and is one of the fundamental properties of nanofluid (Pang et al., 2012).

Also, the optical microscope was used to obtain some morphological information about the powder. An optical micrograph (Figure 4.2b**)** of the colloidal solution dispersed on a glass slide shows the spherical particles, the agglomeration of the nanoparticles, with a diameter of about 1 μm.

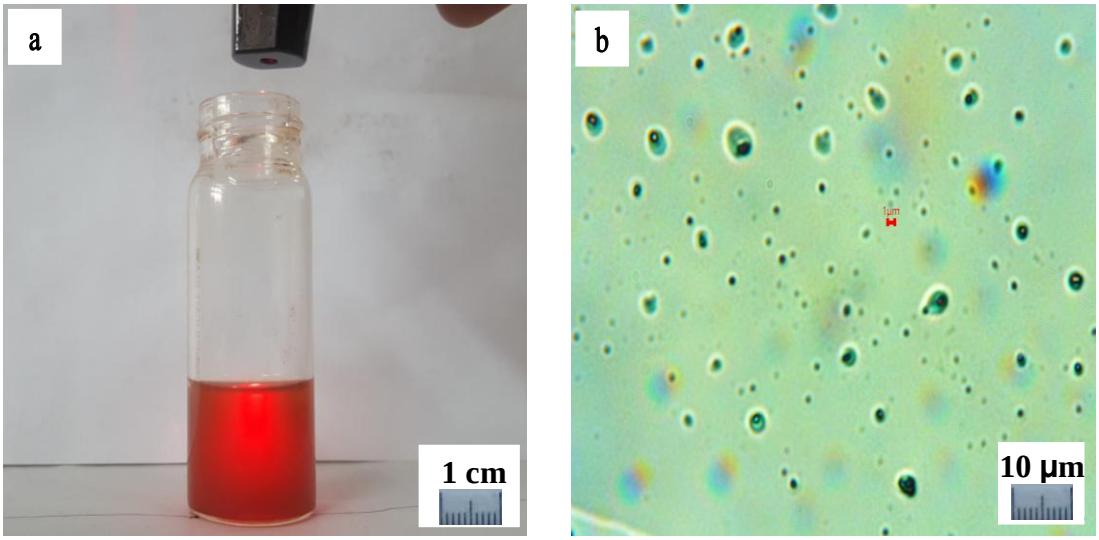

Figure 4.2: Photographs showing optical property and particle morphology: a) scattering of the laser by MNPs colloidal solution, and b) optical micrograph of MNPs deposited on a glass slide

4.2 Chemical Characterization

4.2.1 Ultraviolet-visible (UV-Vis) spectroscopy and Tauc plots

To characterize the band gap energy of the magnetite nanoparticles, UV-Vis spectra of all three samples were recorded. Surface plasmon absorption was observed at a different wavelength for three different samples. However, the samples absorbed nearly at the same wavelength, also corresponding to the literature value, 233 nm (M. Awwad & M. Salem, 2013).

Figure 4.3 shows the UV-Vis spectrum with its corresponding tauc plot for the MNPs-$_{Hex}$. The characteristics surface plasmon absorption of light was found to occur at the wavelength of 224 nm. To calculate energy between O (2p) band to Fe (3d) band for synthesized nanoparticles, the corresponding tauc plot was analyzed.

On plotting $(\alpha h\nu)^2$ with photon energy and extrapolating the straight-line section of the plot to the x-axis ie. taking $(\alpha h\nu)^2 = 0$, the corresponding value of band gap was found to be 4.54 eV. This indicated that MNPs synthesized using hexane as an oil phase had an energy band gap compared to a wide band gap semi-conductor (Shur, 2019). This small change in the absorption wavelength of the sample as well as the band gap from the previously reported value of 233 nm is due to the difference in the size of the particles (Khalil et al., 2012).

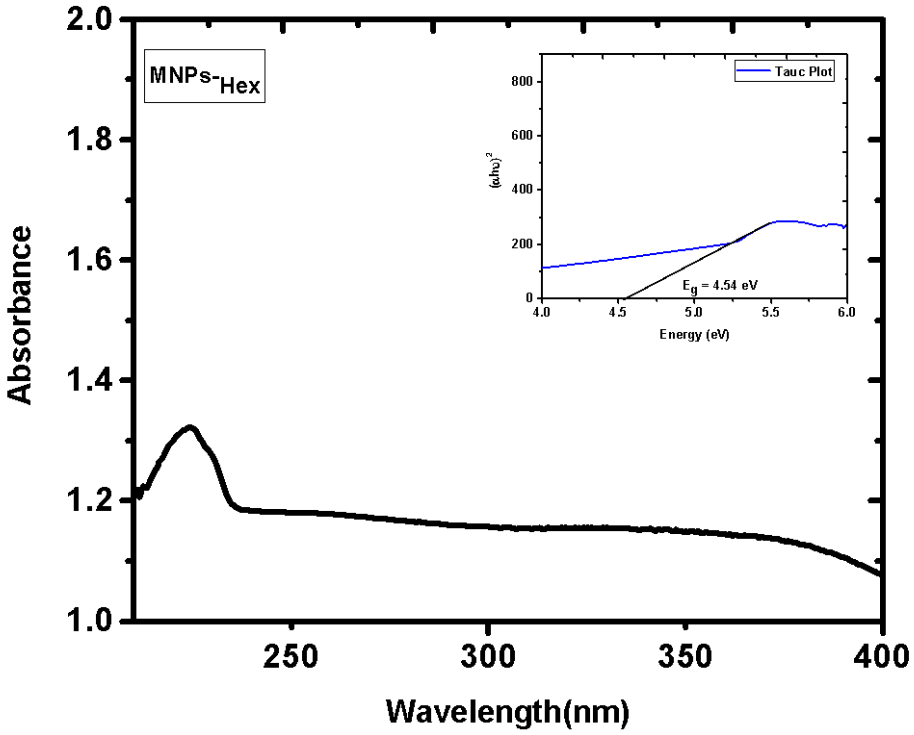

Figure 4.3: Surface plasmon absorption and tauc plot for MNPs-$_{Hex}$

The peak for surface plasmon resonance (SPR) for the MNPs-$_{Must}$ has been recorded at a wavelength of 219 nm. The corresponding band gap energy, hence, can be calculated to be 4.70 eV. It can be thus deducted that the SPR for this sample is lower than that of one reported in the literature and that observed to MNPs-$_{Hex}$ i.e. blue shift. The change in the position of the absorbance peak in UV-Vis spectra compared to MNPs-$_{Hex}$ is due to the change in the particle size called as quantum size effect.

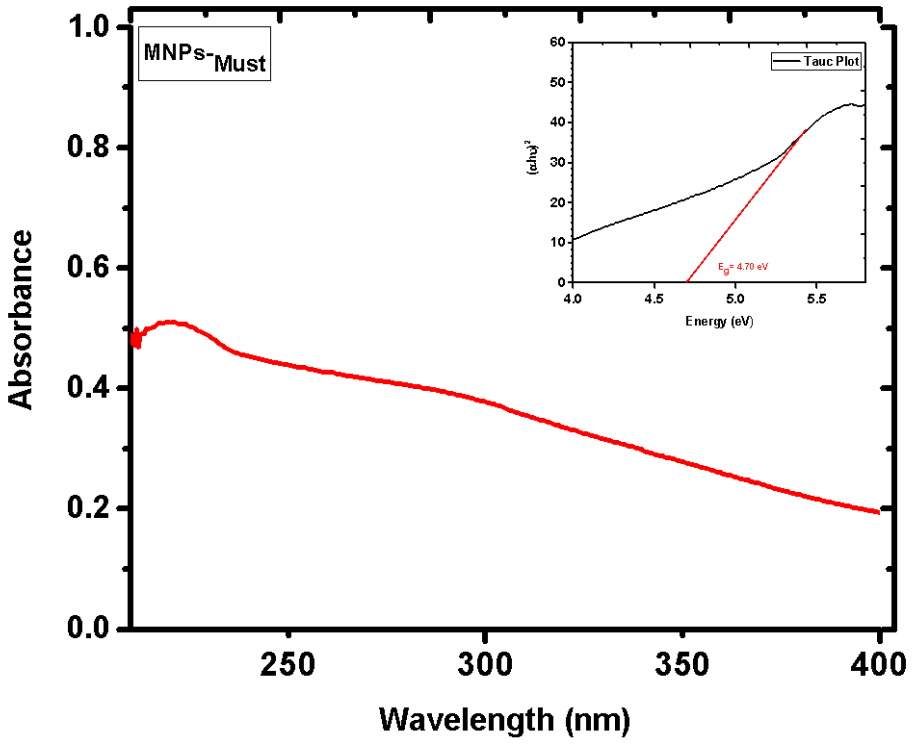

Figure 4.4: Surface plasmon absorption and tauc plot for MNPs-$_{Must}$

Surface plasmon absorption of visible light for MNPs-$_{Soya}$ was found to be at 209 nm (Figure 4.5) and the corresponding band gap energy was calculated to be 5.24 eV. The value of SPR in UV-Vis spectra for MNPs-$_{Soya}$ was at a lower wavelength as compared to both MNPs-$_{Hex}$ and MNPs-$_{Must}$. However, the band gap energy, in this case, was found to be larger than that of two samples MNPs-$_{Hex}$ and MNPs-$_{Must}$. The results so far obtained for three different kinds of MNPs have been summarized in Table 4.1.

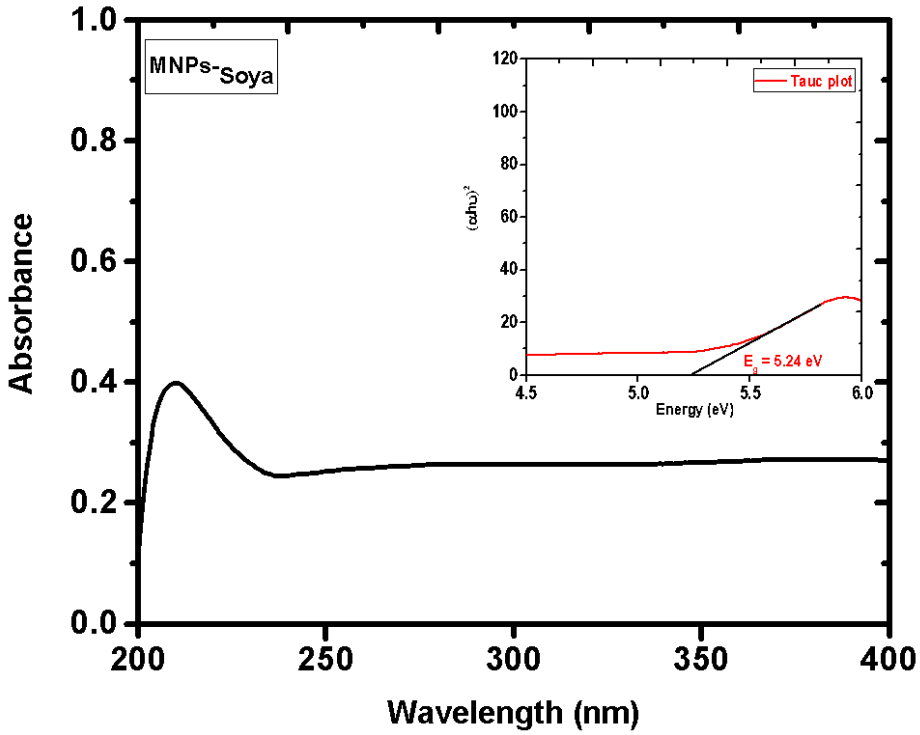

Figure 4.5: Surface plasmon absorption and tauc plot for MNPs-$_{Soya}$

Table 4.1: Surface plasmon absorption and band gap energy of different MNPs

Sample	UV absorbance (nm)	Band gap energy (eV)
MNPs-$_{Hex}$	224	4.54
MNPs-$_{Must}$	219	4.70
MNPs-$_{Soya}$	209	5.24

A decrease in the particle size can be concluded for the shifting of the peak towards a shorter wavelength. The shifting of the absorbance peak towards a shorter wavelength in the case of MNPs-$_{Soya}$ as compared to MNPs-$_{Hex}$ and MNPs-$_{Must}$ indicates a decrease in mean particle size (Khalil et al., 2012). As the SPR absorbance wavelength follow the order of MNPs-$_{Hex}$ > MNPs-$_{Must}$ > MNPs-$_{Soya}$, the mean particle size of MNPs is in the order of MNPs-$_{Hex}$ > MNPs-$_{Must}$ > MNPs-$_{Soya}$. Similarly, as the size of the particles decreases, the corresponding band gap energy increases. Therefore, the highest band gap energy was found in the case of MNPs-$_{Soya}$ as the mean size of the particle is less than that of MNPs-$_{Hex}$ and MNPs-$_{Must}$. Similarly, the broadening of the absorbance peak tells information about the size distribution of the synthesized particle (Alfredo Reyes Villegas et al., 2020).

4.2.2 Fourier transform infrared spectroscopy (FTIR)

FTIR of samples was carried out to characterize the functional groups and bonding nature present in the MNPs. It also provides further information about the interaction of the oil phase on the surface of nanoparticles during synthesis.

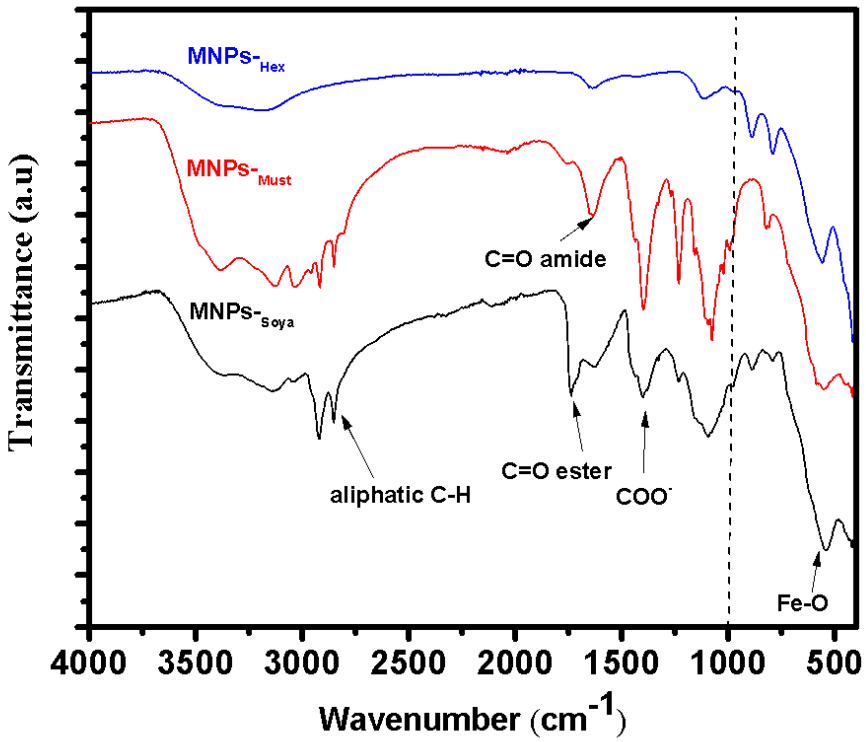

Figure 4.6: FTIR spectra of MNPs synthesized through hexane, mustard oil, soybean oil as oil phase

Figure 4.6 shows the FTIR spectra associated with the MNPs. In FTIR spectra, the absorbance of all bare samples of MNPs at 544 cm^{-1} is due to Fe-O stretching of iron at tetrahedral holes. However, most of the peaks below 1000 cm^{-1} in the IR spectrum were due to the metallic bond (Sakthi Sri et al., 2020). The peak at around 1400 cm^{-1} on sample MNPs-$_{Must}$ and MNPs-$_{Soya}$ is attributed to the asymmetric and symmetric stretching vibration of the COO^{-}group. This result revealed that the C=O group may be bound on the magnetite particle surface. For the sample MNPs-$_{Must}$ the strong amide peak at 1641 cm^{-1}, as well as a weak ester peak at 1760 cm-1, was obtained. However, in MNPs-$_{Soya}$, the peak intensity of amide and ester carbonyl vibrations are

reversed. These were due to the difference in the degree of ammalytion and the hydrolytic reaction of both residual oil phases in a basic medium (Liu et al., 2008).

4.3 Structural Characterization

4.3.1 Study of crystal structure using x-ray diffraction

X-ray diffraction patterns can be used to compare the phase purity, crystallinity and approximate size of crystallite. The XRD patterns of samples are shown in Figure 4.7.

All of the samples show XRD peaks at around 32^o, 37^o,$44\ ^o$,52^o,$58^o$and 63^o (2θ), corresponding to 200, 311, 400, 422, 511 and 440 miller reflection planes, similar to that of MNPs (JCPDS 75-449) indicating that black colored magnetic powders are indeed magnetite. Sharp peak also suggests that Fe_3O_4 NPs have a good crystalline structure (Ma et al., 2003). Peak broadening is consistent with the small particle size. Peak broadening may also be a consequence of defects and some degree of polycrystallinity in magnetite nanoparticles (Stanjek, 2002). The diffraction peak at 37^o (2θ) corresponding to the 311 miller plane family was chosen for calculation of the crystalline size, as it is isolated from other peaks and is relatively sharper (Radoń et al., 2017).

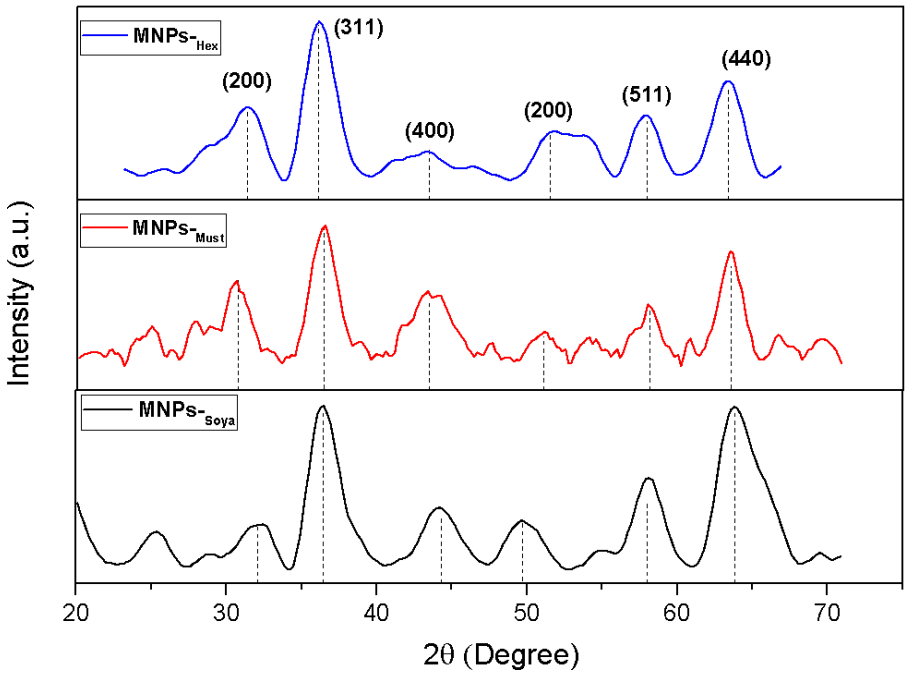

Figure 4.7: XRD patterns of various MNPs samples synthesized using different oil phase

The average crystallite size was calculated using Debye-Scherer's formula,

$$D=\frac{K\lambda}{\beta\, Cos\theta} \qquad (1)$$

Where 'D' is the average crystallite size (nm), 'K' is the shape factor (K = 0.93 for most of the spherical crystals), 'λ' is the wavelength of the X-ray (λ = 0.154 nm for CuKα radiation), 'β' is the full width at half maximum FWHM (radian) and 'θ' is the Bragg's diffraction angle.

Table 4.2: Crystallite size of MNPs prepared by various methods

Sample	FWHM (Radian)	Crystallite Size (nm)
MNPs-$_{Hex}$	0.98105	9.0
MNPs-$_{Must}$	1.42	6.04
MNPs-$_{Soya}$	1.60	5.39

Table 4.2 gives the comparison of the crystalline size of MNPs prepared by various oil phases. The presence of a structural peak in XRD patterns and average crystallite size was calculated as 9.0 nm, 6.04 nm and 5.39 nm for hexane, mustard oil and soybean oil respectively. The average crystallite size of the MNPs was found in the order of MNPs-$_{Hex}$ > MNPs-$_{Must}$ > MNPs-$_{Soya}$ as similar to the result obtained by UV-Vis. Nanocrystalline MNPs were obtained in all cases.

4.3.2 Study of size and morphology using scanning electron microscopy

Scanning electron micrographs recorded and the size distribution curve for the magnetite nanoparticles (MNPs) prepared using different oil phases are shown in Figures 4.8, 4.9 and 4.10 which reveal aggregated spheroids particles with an average diameter of each particle in the nanoscale range. The aggregation of the nanoparticle into clusters might have been caused due to the absence of a capping agent. Similar shaped particles were also prepared previously using the sol-gel method **(** See Figure 4.11**)** (Xu et al., 2007).

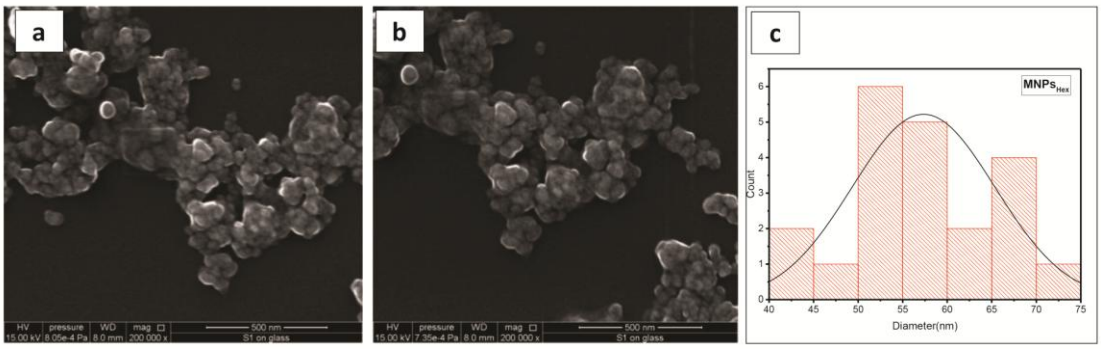

Figure 4.8: SEM micrographs of MNPs-$_{Hex}$: a) High-pressure magnification, b) Low-pressure magnification, and c) Size distribution curve

The morphological characteristics of MNPs using hexane as an oil phase in w/o microemulsion are shown in Figure 4.8a and Figure 4.8b. Both of the micrographs show spheroid morphology of MNPs-$_{Hex}$ which are highly agglomerated to form a cluster having an average diameter of nearly 200 nm. However, the average size of each particle was found to be 57 nm through the size distribution curve (See Figure 4.8c**)**.

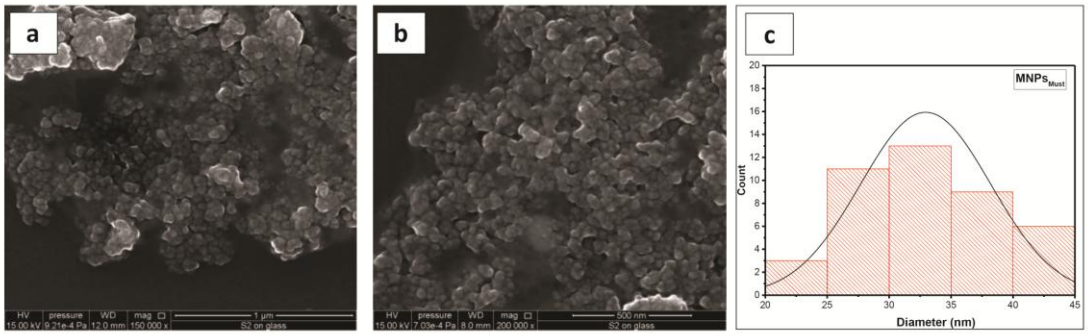

Figure 4.9: SEM micrographs of MNPs-$_{Must}$: a) low magnification, b) high magnification, and c) size distribution curve

Similarly, Figure 4.9 is the SEM micrographs and size distribution curve of MNPs-$_{Must}$ obtained at a low magnification of 1µm (Figure 4.9a) and a high magnification of 500 nm (Figure 4.9b). As like with MNPs-$_{Hex,}$ the shape of the particles was found to be spheroid which is also agglomerated to form a cluster. However, the average diameter of individual particles was 33 nm.

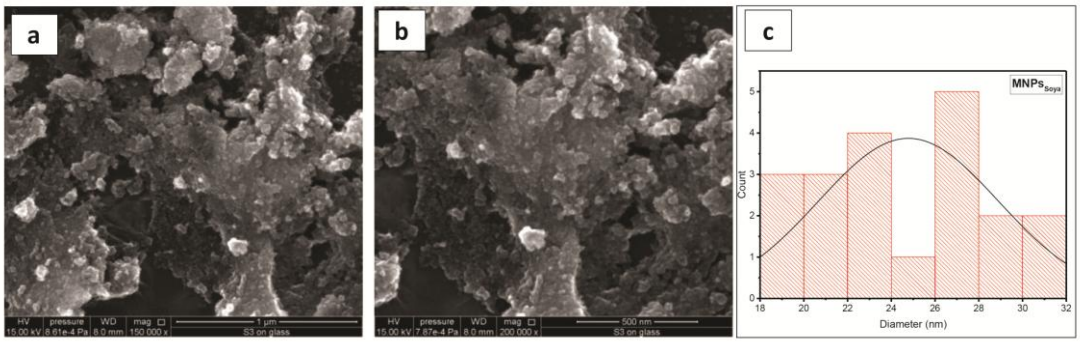

Figure 4.10: SEM micrographs of MNPs-$_{Soya}$: a) Low magnication, b) High magnification, and c) Size distribution curve

Figure 4.10 revel the SEM images as well as the size distribution curve of MNPs-$_{Soya}$. As earlier results, spheroid particles having an average crystallite size of 24 nm with a highly agglomerated cluster can be seen.

SEM images clearly show that nanoparticles can be synthesized using commercial oil as oil phase during the microemulsion technique. The size of the particle can also be varied by using different oil phases. The average size of the particle was also found in the order of MNPs-$_{Hex}$ > MNPs-$_{Must}$ > MNPs-$_{Soya,}$ similar to the results obtained from UV as well as XRD. Here, the variation in average crystallite size is the result of the difference in the size of nanodroplet that has also been mentioned in the literature (Tai & Chen, 2008). But as expected, surface stabilization of the nanoparticle by the oil phase itself was not significantly observed.

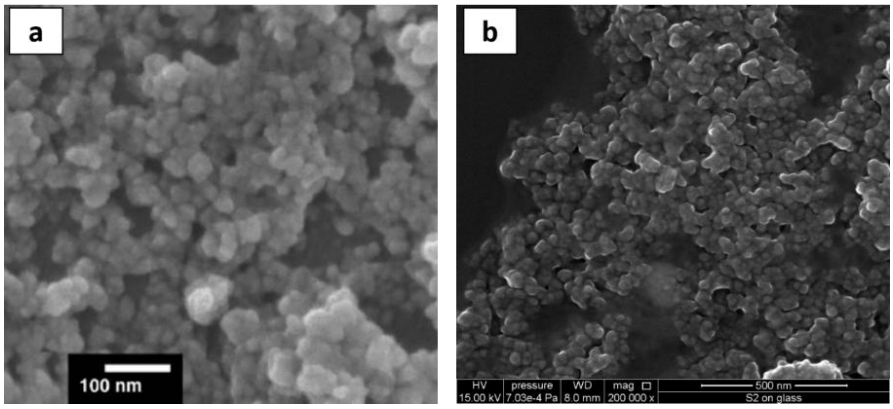

Figure 4.11: Morphology comparison of MNPs: a) prepared by sol-gel method (Xu et al., 2007), and b) prepared using w/o microemulsion

Figure 4.11a and Figure 411b. shows particles morphological photographs of MNPs synthesized through two different methods. Similar spheroid and highly aggregated MNPs were reported by Xu et. al. through the co-precipitation method. No surface capping agents were used in either case.

CHAPTER 5
CONCLUSION AND PERSPECTIVES

This work aims to study the prospect of using edible oil as an organic in w/o microemulsion for the synthesis of magnetite nanoparticles (NPs). Study of the effect of different oil phases on the physical properties of the MNPs by microscopic and spectroscopic methods reveals the following conclusions:

1. The formation of MNPs evident by the Tyndall effect shown by dark magnetite powder suspension.
2. Ultraviolet-visible spectroscopy shows surface plasmon resonance below 225 nm with band gap energies (4.54 eV-5.24 eV) within the range of wide-band semiconductors (2 eV-7 eV) such as SiC, BN.
3. X-ray diffraction of the samples showed their crystalline nature with different crystallites size in the range of 5.4 nm to 9 nm.
4. Fourier transformation infrared spectroscopy showed the presence of Fe-O bond (at 544 cm^{-1}) corresponding with magnetite and COO^- group (1397 cm^{-1}) possibly from the residual oil phases.
5. Scanning electron micrographs of the particles showed larger particles size (but less than 200 nm) due to agglomeration.

This work can be further extended by:

1. The study of the effect of changing the nature of oil, the concentration of surfactant and cosurfactant as well as reaction temperature on the size and morphology of the particles.
2. Performing more experiments to explain the probable presence of the residual oil phase on the surface of the NPs.

References

Ahn, T., Kim, J. H., Yang, H. M., Lee, J. W., & Kim, J. D. (2012). Formation pathways of magnetite nanoparticles by coprecipitation method. *Journal of Physical Chemistry C*, *116*(10), 6069–6076. https://doi.org/10.1021/jp211843g

Al-Jumaili, A., Alancherry, S., Bazaka, K., & Jacob, M. V. (2017). Review on the antimicrobial properties of carbon nanostructures. In *Materials* (Vol. 10, Issue 9, p. 1066). MDPI AG. https://doi.org/10.3390/ma10091066

Alfredo Reyes Villegas, V., Isaías De León Ramírez, J., Hernandez Guevara, E., Perez Sicairos, S., Angelica Hurtado Ayala, L., & Landeros Sanchez, B. (2020). Synthesis and characterization of magnetite nanoparticles for photocatalysis of nitrobenzene. *Journal of Saudi Chemical Society*, *24*(2), 223–235. https://doi.org/10.1016/j.jscs.2019.12.004

Andrade, Â. L., Fabris, J. D., Ardisson, J. D., Valente, M. A., & Ferreira, J. M. F. (2012). Effect of Tetramethylammonium Hydroxide on Nucleation, Surface Modification and Growth of Magnetic Nanoparticles. *Journal of Nanomaterials*. https://doi.org/10.1155/2012/454759

Boholm, M., & Arvidsson, R. (2016). A Definition Framework for the Terms Nanomaterial and Nanoparticle. *NanoEthics*, *10*(1), 25–40. https://doi.org/10.1007/s11569-015-0249-7

Boufas, M., Guellati, O., Harat, A., Momodu, D., Dangbegnon, J., Manyala, N., & Guerioune, M. (2020). Optical and electrochemical properties of iron oxide and hydroxide nanofibers synthesized using new template-free hydrothermal method. *Journal of Nanostructure in Chemistry*, *10*(4), 275–288. https://doi.org/10.1007/s40097-020-00348-8

Bragg, W. H. (1915). The structure of magnetite and the spinels [1]. In *Nature* (Vol. 95, Issue 2386, p. 561). Nature Publishing Group. https://doi.org/10.1038/095561a0

Cheng, F. Y., Su, C. H., Yang, Y. S., Yeh, C. S., Tsai, C. Y., Wu, C. L., Wu, M. T., & Shieh, D. Bin. (2005). Characterization of aqueous dispersions of Fe3O4

nanoparticles and their biomedical applications. *Biomaterials*, *26*(7), 729–738. https://doi.org/10.1016/j.biomaterials.2004.03.016

Choi, W. K., Liew, T. H., Chew, H. G., Zheng, F., Thompson, C. V., Wang, Y., Hong, M. H., Wang, X. D., Li, L., & Yun, J. (2008). A Combined Top-Down and Bottom-Up Approach for Precise Placement of Metal Nanoparticles on Silicon. *Small*, *4*(3), 330–333. https://doi.org/10.1002/smll.200700728

Daou, T. J., Pourroy, G., Bégin-Colin, S., Grenèche, J. M., Ulhaq-Bouillet, C., Legaré, P., Bernhardt, P., Leuvrey, C., & Rogez, G. (2006). Hydrothermal synthesis of monodisperse magnetite nanoparticles. *Chemistry of Materials*, *18*(18), 4399–4404. https://doi.org/10.1021/cm060805r

Deng, H., & Lei, Z. (2013). Preparation and characterization of hollow Fe 3 O 4 /SiO 2 @PEG-PLA nanoparticles for drug delivery. *COMPOSITES PART B*, *54*, 194–199. https://doi.org/10.1016/j.compositesb.2013.05.010

Deshmukh, K. (2019). *Nanotechnology in Ancient Era* (pp. 3–14). Springer, Cham. https://doi.org/10.1007/978-3-319-92399-4_1

Dorfs, D., Krahne, R., Falqui, A., Manna, L., Giannini, C., & Zanchet, D. (2019). Quantum dots: Synthesis and characterization. In *Comprehensive Nanoscience and Nanotechnology* (Vols. 1–5, pp. 17–60). Elsevier. https://doi.org/10.1016/B978-0-12-812295-2.00028-3

Ealias, A. M., & Saravanakumar, M. P. (2017). A review on the classification, characterisation, synthesis of nanoparticles and their application. *IOP Conference Series: Materials Science and Engineering*, *263*(3), 032019. https://doi.org/10.1088/1757-899X/263/3/032019

Eastoe, J., Hollamby, M. J., & Hudson, L. (2006). Recent advances in nanoparticle synthesis with reversed micelles. In *Advances in Colloid and Interface Science*. https://doi.org/10.1016/j.cis.2006.11.009

Estelrich, J., & Antònia Busquets, M. (2018). Iron Oxide Nanoparticles in Photothermal Therapy. *Molecules 2018, Vol. 23, Page 1567*, *23*(7), 1567. https://doi.org/10.3390/MOLECULES23071567

Fato, F. P., Li, D. W., Zhao, L. J., Qiu, K., & Long, Y. T. (2019). Simultaneous Removal of Multiple Heavy Metal Ions from River Water Using Ultrafine Mesoporous Magnetite Nanoparticles. *ACS Omega*, *4*(4), 7543–7549. https://doi.org/10.1021/ACSOMEGA.9B00731/SUPPL_FILE/AO9B00731_SI_001.PDF

Fleet, M. E. (1981). The structure of magnetite. *Acta Crystallographica Section B Structural Crystallography and Crystal Chemistry*, *37*(4), 917–920. https://doi.org/10.1107/s0567740881004597

Frankel, R. B., & Blakemore, R. P. (1989). Magnetite and magnetotaxis in microorganisms. *Bioelectromagnetics*, *10*(3), 223–237. https://doi.org/10.1002/bem.2250100303

Freestone, I., Meeks, N., Sax, M., & Higgitt, C. (2008). The Lycurgus Cup - A Roman nanotechnology. *Gold Bulletin*, *40*(4), 270–277. https://doi.org/10.1007/BF03215599

Gharpure, S., Akash, A., & Ankamwar, B. (2019). A Review on Antimicrobial Properties of Metal Nanoparticles. *Journal of Nanoscience and Nanotechnology*, *20*(6), 3303–3339. https://doi.org/10.1166/jnn.2020.17677

Ghimire, S., Lebek, W., Godehardt, R., Lee, W. I., & Adhikari, R. (2016). Morphology and optical properties of bare and silica coated hybrid silver nanoparticles. *Journal of Nanoscience and Nanotechnology*, *16*(5), 5200–5206. https://doi.org/10.1166/jnn.2016.12155

Giraldo, L., Erto, A., & Moreno-Piraján, J. C. (2013). Magnetite nanoparticles for removal of heavy metals from aqueous solutions: Synthesis and characterization. *Adsorption*, *19*(2–4), 465–474. https://doi.org/10.1007/s10450-012-9468-1

Habte, L., Shiferaw, N., Mulatu, D., Thenepalli, T., Chilakala, R., & Ahn, J. W. (2019). Synthesis of Nano-Calcium Oxide from Waste Eggshell by Sol-Gel Method. *Sustainability 2019, Vol. 11, Page 3196*, *11*(11), 3196. https://doi.org/10.3390/SU11113196

Hamed Sadabadi, A. A. (2015). Application of Magnetite (Fe3O4) Nanoparticles in Hexavalent Chromium Adsorption from Aquatic Solutions. *Journal of Petroleum & Environmental Biotechnology*, *06*(01), 1–3. https://doi.org/10.4172/2157-7463.1000200

Horst, M. F., Coral, D. F., Fernández van Raap, M. B., Alvarez, M., & Lassalle, V. (2017). Hybrid nanomaterials based on gum Arabic and magnetite for hyperthermia treatments. *Materials Science and Engineering C*, *74*, 443–450. https://doi.org/10.1016/j.msec.2016.12.035

Hu, P., Chang, T., Chen, W. J., Deng, J., Li, S. L., Zuo, Y. G., Kang, L., Yang, F., Hostetter, M., & Volinsky, A. A. (2019). Temperature effects on magnetic properties of Fe3O4 nanoparticles synthesized by the sol-gel explosion-assisted method. *Journal of Alloys and Compounds*, *773*, 605–611. https://doi.org/10.1016/J.JALLCOM.2018.09.238

Irshad, K., Khan, M. T., & Murtaza, A. (2018). Synthesis and characterization of transition-metals-doped ZnO nanoparticles by sol-gel auto-combustion method. *Physica B: Condensed Matter*, *543*, 1–6. https://doi.org/10.1016/J.PHYSB.2018.05.006

Jagtap, S., Chopade, P., Tadepalli, S., Bhalerao, A., & Gosavi, S. (2019). A review on the progress of ZnSe as inorganic scintillator. *Opto-Electronics Review*, *27*(1), 90–103. https://doi.org/10.1016/J.OPELRE.2019.01.001

Jeevanandam, J., Barhoum, A., Chan, Y. S., Dufresne, A., & Danquah, M. K. (2018). Review on nanoparticles and nanostructured materials: history, sources, toxicity and regulations. *Beilstein J. Nanotechnol*, *9*, 1050–1074. https://doi.org/10.3762/bjnano.9.98

Jones, R. G., Ober, C. K., Hayakawa, T., Luscombe, C. K., & Stingelin, N. (2020). Terminology of polymers in advanced lithography (IUPAC Recommendations 2020). *Pure and Applied Chemistry*, *92*(11), 1861–1891. https://doi.org/10.1515/PAC-2018-1215/PDF

Karami, H. (2013). Heavy metal removal from water by magnetite nanorods. *Chemical Engineering Journal*, *219*, 209–216. https://doi.org/10.1016/j.cej.2013.01.022

Khalil, M., Ismail, M. I. M., El Ghandoor, H., Zidan, H. M., & Khalil, M. M. H. (2012). Synthesis and Some Physical Properties of Magnetite (Fe 3 O 4) Nanoparticles. *J. Electrochem. Sci*, *7*, 5734–5745. www.electrochemsci.org

Khollam, Y. B., Dhage, S. R., Potdar, H. S., Deshpande, S. B., Bakare, P. P., Kulkarni, S. D., & Date, S. K. (2002). Microwave hydrothermal preparation of submicron-sized spherical magnetite (Fe3O4) powders. *Materials Letters*, *56*(4), 571–577. https://doi.org/10.1016/S0167-577X(02)00554-2

Kodama, R. H. (1999). Magnetic nanoparticles. *Journal of Magnetism and Magnetic Materials*, *200*(1–3), 359–372. https://doi.org/10.1016/S0304-8853(99)00347-9

Kozlovskiy, A. L., Ermekova, A. E., Korolkov, I. V., Chudoba, D., Jazdzewska, M., Ludzik, K., Nazarova, A., Marciniak, B., Kontek, R., Shumskaya, A. E., & Zdorovets, M. V. (2019). Study of phase transformations, structural, corrosion properties and cytotoxicity of magnetite-based nanoparticles. *Vacuum*, *163*, 236–247. https://doi.org/10.1016/j.vacuum.2019.02.029

Latorre, M., & Rinaldi, ; Carlos. (2009). *Applications of Magnetic Nanoparticles in Medicine: Magnetic Fluid Hyperthermia*.

Li, H., & Zhang, L. (2017). Photocatalytic performance of different exposed crystal facets of BiOCl. In *Current Opinion in Green and Sustainable Chemistry* (Vol. 6, pp. 48–56). Elsevier B.V. https://doi.org/10.1016/j.cogsc.2017.05.005

Liang, X., Jia, X., Cao, L., Sun, J., & Yang, Y. (2010). Microemulsion synthesis and characterization of nano-Fe3O4 particles and Fe3O4 nanocrystalline. *Journal of Dispersion Science and Technology*, *31*(8), 1043–1049. https://doi.org/10.1080/01932690903224755

Linh, P. H., Phuc, N. X., Hong, L. V., Uyen, L. L., Chien, N. V., Nam, P. H., Quy, N. T., Nhung, H. T. M., Phong, P. T., & Lee, I. J. (2018). Dextran coated magnetite high

susceptibility nanoparticles for hyperthermia applications. *Journal of Magnetism and Magnetic Materials*, *460*, 128–136. https://doi.org/10.1016/J.JMMM.2018.03.065

Liu, J. F., Zhao, Z. S., & Jiang, G. Bin. (2008). Coating Fe3O4 magnetic nanoparticles with humic acid for high efficient removal of heavy metals in water. *Environmental Science and Technology*, *42*(18), 6949–6954. https://doi.org/10.1021/ES800924C/SUPPL_FILE/ES800924C_SI_001.PDF

Lyubutin, I. S., Lin, C. R., Tseng, Y. T., Spivakov, A., Baskakov, A. O., Starchikov, S. S., Funtov, K. O., Jhang, C. J., Tsai, Y. J., & Hsu, H. S. (2019). Structural and magnetic evolution of Fe x O y @carbon core-shell nanoparticles synthesized by a one-step thermal pyrolysis. *Materials Characterization*, *150*, 213–219. https://doi.org/10.1016/j.matchar.2019.02.022

M. Awwad, A., & M. Salem, N. (2013). A Green and Facile Approach for Synthesis of Magnetite Nanoparticles. *Nanoscience and Nanotechnology*, *2*(6), 208–213. https://doi.org/10.5923/j.nn.20120206.09

Ma?, M., Zhang, Y., Yu, W., Shen, H., Zhang, H., & Gu, N. (2014). Preparation and characterization of magnetite nanoparticles coated by amino silane. *Applied Mechanics and Materials*, *618*, 24–27. https://doi.org/10.4028/www.scientific.net/AMM.618.24

Ma, M., Zhang, Y., Yu, W., Shen, H. Y., Zhang, H. Q., & Gu, N. (2003). Preparation and characterization of magnetite nanoparticles coated by amino silane. *Colloids and Surfaces A: Physicochemical and Engineering Aspects*, *212*(2–3), 219–226. https://doi.org/10.1016/S0927-7757(02)00305-9

Maity, D., Chandrasekharan, P., Yang, C.-T., Chuang, K.-H., Shuter, B., Xue, J.-M., Ding, J., & Feng, S.-S. (2010). Facile synthesis of water-stable magnetite nanoparticles for clinical MRI and magnetic hyperthermia applications. *Nanomedicine*, *5*(10), 1571–1584. https://doi.org/10.2217/nnm.10.77

Majewski, P., & Thierry, B. (2007). Functionalized Magnetite Nanoparticles—Synthesis, Properties, and Bio-Applications. *Critical Reviews in Solid State and Materials Sciences*, *32*(3–4), 203–215. https://doi.org/10.1080/10408430701776680

Makuła, P., Pacia, M., & Macyk, W. (2018). How To Correctly Determine the Band Gap Energy of Modified Semiconductor Photocatalysts Based on UV-Vis Spectra. *Journal of Physical Chemistry Letters*, *9*(23), 6814–6817. https://doi.org/10.1021/ACS.JPCLETT.8B02892/SUPPL_FILE/JZ8B02892_LIVESLIDES.MP4

Malik, M. A., Wani, M. Y., & Hashim, M. A. (2012). Microemulsion method: A novel route to synthesize organic and inorganic nanomaterials. 1st Nano Update. In *Arabian Journal of Chemistry* (Vol. 5, Issue 4, pp. 397–417). Elsevier. https://doi.org/10.1016/j.arabjc.2010.09.027

Mehnath, S., Das, A. K., Verma, S. K., & Jeyaraj, M. (2021). Biosynthesized/green-synthesized nanomaterials as potential vehicles for delivery of antibiotics/drugs. In *Comprehensive Analytical Chemistry* (Vol. 94, pp. 363–432). Elsevier B.V. https://doi.org/10.1016/bs.coac.2020.12.011

Min, Y., Caster, J. M., Eblan, M. J., & Wang, A. Z. (2015). Clinical Translation of Nanomedicine. *Chemical Reviews*, *115*(19), 11147. https://doi.org/10.1021/ACS.CHEMREV.5B00116

Morel, M., Martínez, F., & Mosquera, E. (2013). Synthesis and characterization of magnetite nanoparticles from mineral magnetite. *Journal of Magnetism and Magnetic Materials*, *343*, 76–81. https://doi.org/10.1016/J.JMMM.2013.04.075

Murty, B. S., Shankar, P., Raj, B., Rath, B. B., & Murday, J. (2013). Textbook of Nanoscience and Nanotechnology. In *Textbook of Nanoscience and Nanotechnology*. https://doi.org/10.1007/978-3-642-28030-6

Muthu, S., Raju, V., Gopal, V. B., Gunasekaran, A., Narayan, K. S., Malairaj, S., Lakshmikanthan, M., Duraisamy, N., Krishnan, K., & Perumal, P. (2019). A rapid synthesis and antibacterial property of selenium nanoparticles using egg white lysozyme as a stabilizing agent. *SN Applied Sciences*, *1*(12), 1–9. https://doi.org/10.1007/S42452-019-1509-X/FIGURES/7

Niculescu, A. G., Chircov, C., & Grumezescu, A. M. (2021). Magnetite nanoparticles: Synthesis methods – A comparative review. *Methods*. https://doi.org/10.1016/J.YMETH.2021.04.018

Nkurikiyimfura, I., Wang, Y., Safari, B., & Nshingabigwi, E. (2020). Temperature-dependent magnetic properties of magnetite nanoparticles synthesized via coprecipitation method. *Journal of Alloys and Compounds*, *846*, 156344. https://doi.org/10.1016/J.JALLCOM.2020.156344

Pang, C., Jung, J.-Y., Lee, J. W., & Kang, Y. T. (2012). Thermal conductivity measurement of methanol-based nanofluids with Al 2 O 3 and SiO 2 nanoparticles. *International Journal of Heat and Mass Transfer*, *55*, 5597–5602. https://doi.org/10.1016/j.ijheatmasstransfer.2012.05.048

Prilepskii, A. Y., Fakhardo, A. F., Drozdov, A. S., Vinogradov, V. V., Dudanov, I. P., Shtil, A. A., Bel'Tyukov, P. P., Shibeko, A. M., Koltsova, E. M., Nechipurenko, D. Y., & Vinogradov, V. V. (2018). Urokinase-Conjugated Magnetite Nanoparticles as a Promising Drug Delivery System for Targeted Thrombolysis: Synthesis and Preclinical Evaluation. *ACS Applied Materials & Interfaces*, *10*(43), 36764–36775. https://doi.org/10.1021/ACSAMI.8B14790

Radoń, A., Drygała, A., Hawełek, Ł., & Łukowiec, D. (2017). Structure and optical properties of Fe3O4 nanoparticles synthesized by co-precipitation method with different organic modifiers. *Materials Characterization*, *131*, 148–156. https://doi.org/10.1016/j.matchar.2017.06.034

Rashid, M., Price, N. T., Gracia Pinilla, M. Á., & O'Shea, K. E. (2017). Effective removal of phosphate from aqueous solution using humic acid coated magnetite nanoparticles. *Water Research*, *123*, 353–360. https://doi.org/10.1016/j.watres.2017.06.085

Sakthi Sri, S. P., Taj, J., & George, M. (2020). Facile synthesis of magnetite nanocubes using deep eutectic solvent: an insight to anticancer and photo-Fenton efficacy. *Surfaces and Interfaces*, *20*, 100609. https://doi.org/10.1016/J.SURFIN.2020.100609

Saleh, T. A. (2020). Nanomaterials: Classification, properties, and environmental toxicities. In *Environmental Technology and Innovation* (Vol. 20, p. 101067). Elsevier B.V. https://doi.org/10.1016/j.eti.2020.101067

Salem, M., Xia, Y., Allan, A., Rohani, S., & Gillies, E. R. (2015). Curcumin-loaded, folic acid-functionalized magnetite particles for targeted drug delivery. *RSC Advances*, *5*(47), 37521–37532. https://doi.org/10.1039/C5RA01811K

Salvador, M., Gutiérrez, G., Noriega, S., Moyano, A., Blanco-López, M. C., & Matos, M. (2021). Microemulsion Synthesis of Superparamagnetic Nanoparticles for Bioapplications. *International Journal of Molecular Sciences 2021, Vol. 22, Page 427*, *22*(1), 427. https://doi.org/10.3390/IJMS22010427

sara shaker, shirzad zafarian, shilpa chakra, venkateswawa rao. (2013). Preparation and Characterization of Magnetite Nanoparticles By Sol-Gel Method for Water Treatment. *International Journal of Innovative Research in Science, Engineering and Technology*, *2*(7), 2969–2972. https://doi.org/10.1016/j.arabjc.2010.06.061

Satter, S. S., Hoque, M., Rahman, M. M., Mollah, M. Y. A., & Bin Hasan Susan, M. A. (2014). An approach towards the synthesis and characterization of ZnO@Ag core@shell nanoparticles in water-in-oil microemulsion. *RSC Advances*, *4*(39), 20612–20615. https://doi.org/10.1039/C4RA01046A

Schaming, D., & Remita, H. (2015). Nanotechnology: from the ancient time to nowadays. *Foundations of Chemistry*, *17*(3), 187–205. https://doi.org/10.1007/s10698-015-9235-y

Schmitz-Antoniak, C. (2015). X-ray absorption spectroscopy on magnetic nanoscale systems for modern applications. *Reports on Progress in Physics*, *78*(6). https://doi.org/10.1088/0034-4885/78/6/062501

Schwaminger, S. P., Bauer, D., Fraga-García, P., Wagner, F. E., & Berensmeier, S. (2017). Oxidation of magnetite nanoparticles: impact on surface and crystal properties. *CrystEngComm*, *19*(2), 246–255. https://doi.org/10.1039/c6ce02421a

Sharifi, S., Behzadi, S., Laurent, S., Forrest, M. L., Stroeve, P., & Mahmoudi, M. (2012). Toxicity of nanomaterials. *Chemical Society Reviews*, *41*(6), 2323–2343. https://doi.org/10.1039/c1cs15188f

Shen, X., Chi, Y., & Xiong, K. (2019). The effect of heavy metal contamination on humans and animals in the vicinity of a zinc smelting facility. *PLOS ONE*, *14*(10), e0207423. https://doi.org/10.1371/JOURNAL.PONE.0207423

Shur, M. (2019). Wide band gap semiconductor technology: State-of-the-art. *Solid-State Electronics*, *155*, 65–75. https://doi.org/10.1016/J.SSE.2019.03.020

Singh, P., & Upadhyay, C. (2018). Fine tuning of size and morphology of magnetite nanoparticles synthesized by microemulsion. *AIP Conference Proceedings*, *1953*(1), 030051. https://doi.org/10.1063/1.5032386

Stanjek, H. (2002). XRD peak migration and apparent shift of cell-edge lengths of nano-sized hematite, goethite and lepidocrocite. *Clay Minerals*, *37*(4), 629–638. https://doi.org/10.1180/0009855023740065

Sun, S., & Zeng, H. (2002). Size-controlled synthesis of magnetite nanoparticles. *Journal of the American Chemical Society*, *124*(28), 8204–8205. https://doi.org/10.1021/ja026501x

Szunerits, S., Spadavecchia, J., & Boukherroub, R. (2014). Surface plasmon resonance: Signal amplification using colloidal gold nanoparticles for enhanced sensitivity. *Reviews in Analytical Chemistry*, *33*(3), 153–164. https://doi.org/10.1515/REVAC-2014-0011/ASSET/GRAPHIC/REVAC-2014-0011_FIG2.JPG

Tabesh, S., Davar, F., & Loghman-Estarki, M. R. (2018). Preparation of γ-Al2O3 nanoparticles using modified sol-gel method and its use for the adsorption of lead and cadmium ions. *Journal of Alloys and Compounds*, *730*, 441–449. https://doi.org/10.1016/J.JALLCOM.2017.09.246

Tadic, M., Panjan, M., Vucetic Tadic, B., Lazovic, J., Damnjanovic, V., ⊞⊞ M. K., & ⊞⊞⊞ L. K. (2019). Magnetic properties of hematite ($\alpha - Fe_2O_3$) nanoparticles synthesized by sol-gel synthesis method: The influence of particle size and particle size distribution. *Journal of ELECTRICAL ENGINEERING*, *70*, 71–76. https://doi.org/10.2478/jee-2019-0044

Tai, C. Y., & Chen, C. kuang. (2008). Particle morphology, habit, and size control of CaCO3 using reverse microemulsion technique. *Chemical Engineering Science*, *63*(14), 3632–3642. https://doi.org/10.1016/j.ces.2008.04.022

Takai, Z. I., Mustafa, M. K., Asman, S., & Sekak, K. A. (2019). Preparation and characterization of magnetite (Fe3O4) nanoparticles by sol-gel method. *International Journal of Nanoelectronics and Materials*, *12*(1), 37–46.

Tian, Y., Yu, B., Li, X., & Li, K. (2011). Facile solvothermal synthesis of monodisperse Fe3O4 nanocrystals with precise size control of one nanometre as potential MRI contrast agents. *Journal of Materials Chemistry*, *21*(8), 2476–2481. https://doi.org/10.1039/c0jm02913k

Torres-Gómez, N., Nava, O., Argueta-Figueroa, L., García-Contreras, R., Baeza-Barrera, A., & Vilchis-Nestor, A. R. (2019). Shape tuning of magnetite nanoparticles obtained by hydrothermal synthesis: Effect of temperature. *Journal of Nanomaterials*, *2019*. https://doi.org/10.1155/2019/7921273

Toumey, C. (2009). Plenty of room, plenty of history. In *Nature Nanotechnology* (Vol. 4, Issue 12, pp. 783–784). Nature Publishing Group. https://doi.org/10.1038/nnano.2009.357

Trivedi, N. S., Pandhare, G. G., Trivedi, N., Pathrabe, R., Dawande, S. D., & Tech, M. (2007). Adsorption of cadmium (ii) and lead (ii) from a stock solution using neem leaves powder as a low-cost adsorbent. *International Journal of Innovative Research in Science, Engineering and Technology (An ISO*, *3297*. www.ijirset.com

Wei, X., Sugumaran, P. J., Peng, E., Liu, X. L., & Ding, J. (2017). Low-Field Dynamic Magnetic Separation by Self-Fabricated Magnetic Meshes for Efficient Heavy Metal Removal. *ACS Applied Materials and Interfaces*, *9*(42), 36772–36782. https://doi.org/10.1021/ACSAMI.7B10549/SUPPL_FILE/AM7B10549_SI_003.AVI

Weidenfeller, B., Höfer, M., & Schilling, F. (2002). Thermal and electrical properties of magnetite filled polymers. *Composites Part A: Applied Science and Manufacturing*, *33*(8), 1041–1053. https://doi.org/10.1016/S1359-835X(02)00085-4

Xin, X., Wei, Q., Yang, J., Yan, L., Feng, R., Chen, G., Du, B., & Li, H. (2012). Highly efficient removal of heavy metal ions by amine-functionalized mesoporous Fe 3O 4 nanoparticles. *Chemical Engineering Journal*, *184*, 132–140. https://doi.org/10.1016/j.cej.2012.01.016

Xu, J., Yang, H., Fu, W., Du, K., Sui, Y., Chen, J., Zeng, Y., Li, M., & Zou, G. (2007). Preparation and magnetic properties of magnetite nanoparticles by sol-gel method. *Journal of Magnetism and Magnetic Materials*, *309*(2), 307–311. https://doi.org/10.1016/j.jmmm.2006.07.037

Yadav, B. Sen, Singh, R., Vishwakarma, A. K., & Kumar, N. (2020). Facile Synthesis of Substantially Magnetic Hollow Nanospheres of Maghemite (γ-Fe2O3) Originated from Magnetite (Fe3O4) via Solvothermal Method. *Journal of Superconductivity and Novel Magnetism 2020 33:7*, *33*(7), 2199–2208. https://doi.org/10.1007/S10948-020-05481-7

Yadav, V. K., Ali, D., Khan, S. H., Gnanamoorthy, G., Choudhary, N., Yadav, K. K., Thai, V. N., Hussain, S. A., & Manhrdas, S. (2020). Synthesis and Characterization of Amorphous Iron Oxide Nanoparticles by the Sonochemical Method and Their Application for the Remediation of Heavy Metals from Wastewater. *Nanomaterials 2020, Vol. 10, Page 1551*, *10*(8), 1551. https://doi.org/10.3390/NANO10081551

Yoshida, M., & Lahann, J. (2008). Smart nanomaterials. *ACS Nano*, *2*(6), 1101–1107. https://doi.org/10.1021/nn800332g

Yunus, Z. M., Al-Gheethi, A., Othman, N., Hamdan, R., & Ruslan, N. N. (2020). Removal of heavy metals from mining effluents in tile and electroplating industries using honeydew peel activated carbon: A microstructure and techno-economic analysis. *Journal of Cleaner Production*, *251*, 119738. https://doi.org/10.1016/J.JCLEPRO.2019.119738

Zeng, Y., Yu, M., Meng, Y., Fang, P., Lu, X., & Tong, Y. (2016). Iron-Based Supercapacitor Electrodes: Advances and Challenges. In *Advanced Energy Materials* (Vol. 6, Issue 24). Wiley-VCH Verlag. https://doi.org/10.1002/aenm.201601053